Universidad de La Laguna

Facultad de Física

Máster Universitario en Astrofísica

Trabajo Fin de Máster

Discovering and validating exoplanets from TESS using archival radial velocities

Jaume Orell Miquel

Curso académico 2019-20

Tutor: Rafael Luque
Cotutor: Enric Pallé

Contents

Resumen

La exoplanetología es a día de hoy una rama consolidada de la astrofísica con más de 4 000 exoplanetas descubiertos. Por eso, próximas misiones como CHEOPS se centrarán en observar planetas ya descubiertos, mejorando el conocimiento que tenemos sobre ellos. Pero por otra parte, hay que determinar cuáles son los mejores candidatos para futuros estudios, especialmente para el estudio de sus atmósferas. Aquí es donde entra en juego Transiting Exoplanet Survey Satellite (TESS). TESS es un telescopio espacial que desde abril de 2018 orbita la Tierra y tiene como misión observar todo el cielo durante dos años, distribuido en sectores y cada uno durante 27 días. Tiene como objetivo detectar planetas alrededor de las estrellas más brillantes y cercanas que son las idóneas para futuras observaciones, ya sean fotométricas o espectroscópicas, desde tierra o el espacio, para caracterizar en detalle sus propiedades e incluso sus atmósferas.

El método de detección que utiliza el telescopio espacial TESS es el de tránsito. Cuando el planeta pasa enfrente de la estrella, el brillo que se recibe disminuye levemente, produciendo un tránsito o eclipse. Cuando se registra la evolución del brillo de la estrella con el tiempo, lo que se denomina curva de luz, permite detectar estos tránsitos que se repiten de forma periódica. A partir de la curva de luz no solo se puede extraer el periodo de rotación del planeta sino que a través de la profundidad del tránsito, y conociendo el radio de la estrella, se puede determinar con gran precisión el radio del planeta (Ec. 1). Este método no permite la determinación de la masa del planeta, para ello se utiliza conjuntamente el método de velocidades radiales. Éste se basa en medir por efecto Doppler el movimiento en la línea de visión que produce el planeta sobre la estrella. Las oscilaciones en los valores de velocidad radial (RV) se pueden ajustar a modelos planetarios y así obtener la semi-amplitud K de la señal que permite calcular una cota mínima a la masa (Ec. 5). Sólo si se dispone de medidas fotométricas, se puede conocer la inclinación de la orbita y así conocer el valor exacto de la masa del planeta. Si se conoce la masa y el radio y por ende su densidad permite saber si es rocoso o gaseoso y aumentar el conocimiento sobre el nuevo planeta. En este trabajo se han combinado los datos fotométricos de TESS con medidas de RV de archivo.

El paso previo al flujo de trabajo que realicé en cada sector de TESS fue la recopilación de medidas de velocidades radiales. Así, pude crear una base de datos de unas 290 000 observaciones de casi cinco mil estrellas observadas con HARPS, HIRES o HARPS-N, espectrógrafos de alta resolución y estabilidad. Entonces busqué en qué sectores estas estrellas serían observadas por TESS y así, para cada sector, conocer cuáles eran los posibles candidatos a albergar exoplanetas.

El flujo de trabajo para analizar cada sector fue el mismo. Unos días antes de la publicación de los datos fotométricos hago un periodograma generalizado de Lomb-Scargle (GLS) de las RV de las estrellas que se observaran. Así se ve si hay periodicidades en los datos que puedan ser debidas a un exoplaneta que orbita la estrella. Este análisis permite hacer una primera criba de las estrellas que ya tienen planetas descubiertos y donde por tanto no sería raro encontrar tránsitos en sus curvas de luz.

Una vez están disponibles los datos del sector, obtengo las curvas de luz mediante la herramienta TESScut utilizando el código de Python `tesseract`. Éstas se analizan con el algoritmo `Transit Least Squares` (TLS) en busca de tránsitos. En unos minutos se pueden revisar visualmente los resultados de todas las estrellas analizadas con TLS para ver si alguna tiene eclipses. El problema es que todo este proceso se aplica de forma generalizada y puede ser que alguna pase inadvertida y no se detecte. Por esto, después de cada sector compruebo la lista de objetos de interés de TESS

o TOIs. Uno de los equipos de TESS del MIT se encarga de buscar tránsitos en todas las estrellas del sector y alerta de las que encuentra que tienen eventos similares a los de tránsitos planetarios.

Si se da que para alguna de las estrellas que tengo velocidades radiales se encuentran tránsitos, entonces realizo un análisis más en detalle de sus datos utilizando la librería de Python `juliet`. `juliet` permite hacer ajustes de fotometría, RV o ambos a la vez de modelos planetarios. Además, calcula la evidencia bayesiana del modelo que permite una comparación entre los modelos explorados.

En los sectores analizados en este trabajo, que fueron del 17 al 23, TESS encontró 356 nuevos candidatos de los cuales sólo de 3 disponía de velocidades radiales en los archivos. Los detalles del número de estrellas analizadas se muestran en la Tabla 2. Así, los resultados que se presentan en el trabajo son el estudio y caracterización de los candidatos a planetas TOI 1718, 1827 y 1611.

TOI 1718 es una estrella que se observó durante el Sector 20 y de la que se alertaron tránsitos con un período de 5.58 días y que corresponderían a un planeta con un radio de $\sim 4 R_\oplus$. La estrella estaba en la base de datos porque HIRES la observó 3 veces, pero la cantidad de medidas es insuficiente para calcular bien el GLS. Busqué más medidas en otros archivos pero no obtuve resultados útilies. Por esto propuse observarla con HARPS-N pero las condiciones meteorológicas adversas lo impidieron. Sin más medidas que la fotometría de TESS no se puede confirmar el descubrimiento de este planeta, aunque por la consistencia de la profundidad de los tránsitos y la forma de éstos no da indicios de que sea un falso positivo. El resultado del análisis de la curva de luz con `juliet`, mostrado en Fig. 3, sugiere la presencia de un planeta alrededor de TOI 1718 con un radio de $4.04^{+0.09}_{-0.07} R_\oplus$.

TOI 1827 es una enana roja que se observó durante el Sector 23 y se detectaron tránsitos cada 1.46 días correspondientes a un planeta de $1.3 R_\oplus$. En este caso dispongo de 12 medidas de HARPS y 62 de HIRES, cuyo análisis no muestra ninguna señal significativa en el GLS. El análisis conjunto de RV y fotometría permite obtener parámetros fotométricos consistentes con los alertados, y con menores errores, pero debido a la precisión de las RVs las incertidumbres en la masa del planeta son mayores. El ajuste con `juliet` confirma la presencia de una super-Tierra de $1.39^{+0.06}_{-0.05} R_\oplus$ y $1.2 \pm 0.4 M_\oplus$. Con observaciones no públicas del espectrógrafo CARMENES se ha obtenido de forma independiente un valor para K mayor al límite superior que obtengo.

TOI 1611 es el principal resultado de este trabajo. Fue observada durante los Sectores 18, 19 y 20 y se alertó de un candidato con un periodo de 16.2 días y un radio de $2.5 R_\oplus$. Originalmente solo disponía de 6 RV de HIRES pero debido a la colaboración con otro grupo de investigación, que también reportó su descubrimiento, al final obtuve 67 medidas tomadas con el espectrógrafo SOPHIE. Los GLS de las RVs muestran un pico a 16.2 días confirmando la presencia del planeta. A parte, presentan varios picos significativos a 27, 32 y 35 días para los que después de un largo análisis no pude determinar con certeza su naturaleza. Los parámetros del planeta se extrajeron del análisis conjunto de las RV y fotometría con `juliet` utilizando un modelo de 1 planeta y con procesos gaussianos (GP) para explicar las sistemáticas en las RVs. Así se pudo confirmar y caracterizar el planeta determinando una masa de $19 \pm 4 M_\oplus$ y un radio de $2.13^{+0.09}_{-0.07} R_\oplus$. TOI 1611b es un planeta sub-neptuniano rocoso con una composición similar al de la Tierra, según se extrae de Fig. 15. Los resultados del análisis de este planeta formarán parte de un artículo científico en la revista Astronomy & Astrophysics del que participo como segundo autor.

1 Introduction

Exoplanetology is nowadays a consolidated branch of the astrophysics. From the Ancient Greece with the philosophers Democritus and Epicurus to the 2019 Nobel Prize awarded to the astrophysicists Michel Mayor and Didier Queloz, more than 4 000 exoplanets have been discovered. At its beginnings, it was focused on prove and discover planets outside the Solar System. Statistically, we know now that each star we see in our Galaxy has at least one planet. So, the main objective is changing from discover more exoplanets to study and characterize the observed ones. The amount of discovered planets allows us to do statistics about their properties and comprehend more about the planets' diversity. It has been proven that our System is not the only one but we want to learn how frequent are the rocky and gaseous planets or the Earth-sized planets out there, particularly the ones in the habitable zone, where liquid water could exist.

Exoplanet characterization starts with the determination of the radius and the mass, because without them it is not possible to know more about its composition or atmospheric properties. The good results from *CoRoT* and *Kepler* missions detecting transiting planets have led to spacecrafts dedicated to re-observe the known planets and improve its physical parameters like *CHEOPS* mission. The link between the past and the future of exoplanetology is *TESS*.

The most successful methods to discover exoplanets are the transit and the radial velocity techniques, which are the ones used in this work and I will further explain. However, the radial velocity method is based on the Doppler effect and it requires an accuracy in the measurements that is only feasible for relatively bright stars from ground telescopes. The main goal of TESS is to provide accurate photometry observations of nearby and bright stars that will allow a full characterization of their transiting planets with telescopes from ground.

1.1 *TESS*: Transiting Exoplanet Survey Satellite

The Transiting Exoplanet Survey Satellite or *TESS* is a space telescope in collaboration between MIT and NASA launched on April 18, 2018. Initial TESS' mission is a 2-years full sky survey searching for transiting planets, first year observed the southern ecliptic hemisphere and now is finishing to observe the northern. Each ecliptic hemisphere is divided in thirteen regions called sectors. Each sector is a sky strip of 96º x 24º observed by 4 aligned cameras of four 2k x 2k CCDs where each camera covers a squared area of 24º. The center of camera number 4 is pointing to the same position to get a one-year observation region. These ones will coincide with the James Webb Space Telescope (JWST) continuous viewing zone.

Sectors are observed for 27 days (two complete orbits around Earth) in a cadence of 30 min producing Full Frame Images (FFI), but more than 200 000 stars will be observed in a 2min cadence in order to catch short period planets. This targets are mainly nearby, bright stars. TESS is designed to be sensitive to wavelengths from 600 to 1 000nm and to observe stellar spectral types from F5 to M6.

TESS is searching (and finding) planets in nearby and bright stars because that ones are the best candidates for follow-up characterization from ground and space. TESS will produce a 'catalog' of the best planets to observe with JWST (for atmospheric analysis) and to characterize with missions like CHEOPS or the new generation of 30 meters-class telescopes. TESS' scientific objective is to find 50 exoplanets with radii less than $4R_\oplus$. 46 TESS planets have been confirmed to date and there are more than 500 candidates with $R_p < 4R_\oplus$ waiting for their validation.

1.2 Transit photometry method

TESS planet detections are based on the transit method. It is for long the most successful technique to date with more than 3 000 discovered planets. This method is based on regular and accurate photometric observations of a star hoping to catch the precise moment when an exoplanet crosses in front of the star.

The plot of photometry over time is called light curve. When a planet transits in front of the star, it blocks a region of the stellar disk producing a drop in the received flux. But one single event is not enough to claim a discovery. Two transits are required at least to determine the orbital period P and one more, a transit prediction, that corroborates it.

Photometric data can provide some stellar and planetary parameters but the main one for characterization is the transit depth ΔF. It is the flux difference between the star alone and the star when the planet is in front. ΔF can be calculate as the ratio of areas of the planet and the star, assuming spherical shapes for both and a negligible flux from the planet.

$$\Delta F \simeq \left(\frac{R_p}{R_\star}\right)^2 \tag{1}$$

So, the transit method can give the radius of the exoplanet R_p, if $R_\star$ is known, but the method is blind to the other important planet parameter: the mass. Mass can be estimate from statistical methods based on the radius and the orbital semi-major axis, but it is just a prediction. The confirmation of the planetary mass requires observations with other methods and the most common is the Doppler effect measurements.

But the transiting method has some drawbacks. It requires a continuous observation with an optimum cadence to be able to detect the transits. There are some ground telescopes surveying big celestial regions for long time but they are limited by day/night cycle. For these reasons, the most efficient missions which have almost done all the discoveries are the space ones such as CoRoT, Kepler or TESS. With space telescopes the uninterrupted observations can be longer, so the probability increases. Even so, the limitation on sustained observation and the transit probability are still there and that produces a bias over the period of the discovered exoplanets, the ones with shortest periods are favored.

The main disadvantage of the transiting method is that the star, the planet and Earth must be aligned. The geometric probability to observe a planet transiting in a given random-oriented system can be calculated as

$$p_{transit} = \frac{R_\star}{a} \approx 0.005 \left(\frac{R_\star}{R_\odot}\right)\left(\frac{1AU}{a}\right) \tag{2}$$

and for a concrete planet with a R_p radius and taking account of its eccentricity e it is

$$p_{transit} = \left(\frac{R_\star \pm R_p}{a}\right)\left(\frac{1}{1-e^2}\right) \tag{3}$$

Equation 3 shows that planets with non circular orbits ($e > 0$) are more likely to transit. From Eq. 2 it is easy to see that the probability to find a system like Earth-Sun is only 0.5 %. If 200 Earth-Sun alike systems were observed, we hope to detect only 1 of them. Only for systems with Jupiter-size planets that orbits very close to the star, it increases to $\sim$10%.

Also, the probability to catch the transits of a correctly oriented system at any given moment takes part and it can be estimate as $p_{eclipse} \approx t_T/P$. It is clear that planets with shortest periods are more favored even without considering the observational difficulties. The highest probabilities are of 5-8% for ultrashort period planets and for an Earth-Sun alike system is about 0.15%.

At last, to estimate the total probability of observing a planet we need to multiply these probabilities with the abundance of detectable ones. After all these discouraging numbers, one more have to be considered. The used instruments have to had enough precision to detect the flux's variation during the transits. Earth's eclipses produce a $\Delta F \simeq 8.4 \cdot 10^{-5}$ and Jupiter's ones about $1.1 \cdot 10^{-2}$. For these, the continued observations from space telescopes, like TESS, maximizes the probabilities.

In addition, not all the regular decreases in the stellar flux are due to a transiting planet, there are other explanations. These other events that produce a similar exoplanet signature are called false positive. Up to a 70% of the stars in the Milky Way are in multiple systems. When one star passes in front of the other there is a drop in the total flux of the system like a planetary transit. They can be easily distinguished based on inconsistencies in transit depths and the presence of strong secondary eclipses. Another source of false positives can be the the stellar activity. Starspots, like sunspots, are regions of less brightness that spin at the stellar rotation period, until they disappear. So, their effect over a short-time light curve will be very similar to an exoplanet. Future photometric observations predicting next transits or activity measurements could solve the false alarms. To date, more than 400 TESS' planetary candidates have been classified as false positives.

1.3 Radial velocity method

As I mentioned, a complete characterization of the planet can not be done only with the transiting method. The radial velocity method can derive a lower limit for mass but with the inclination of the orbit, which is a photometry parameter, the true mass can be measured. With the two methods, all the characteristics of the planet can be set.

This method is based on measuring the Doppler effect over the stars' spectra produced by displacements of the star in the line of sight. These displacements are done by the star companions, which may be planets or other celestial objects. Unlike the transiting method, the radial velocity one do not require an exact alignment with the planetary system but the Doppler effect is maximum when the system is observed edge-on and are zero, undetectable, when it is face-on.

The radial velocities (RVs) are calculated using the Doppler's equation, $\Delta\lambda/\lambda_0 = v_r/c$, and as many lines as possible are used to measure the $\Delta\lambda$ for each spectrum. But data must be subtracted from unwanted effects that are some orders bigger than the ones produced by a planet, such as Earth's rotation and revolution. In some cases, planet's signals are near the limits of instrumental detection. Only the massive (compared to the mass' star) or the closest ones are relatively easy to detect. The movement that an Earth-size planet do to a Sun-type star is less than 10cm/s. For these reasons, high resolution spectrographs are used to get spectra and the best are the isolated ones because obtain more precise and stable measurements over long periods of time. Current spectrographs such as HARPS can achieve accuracies of 1m/s but it is close to 10cm/s with ESPRESSO.

Like in the transiting method, it needs observations spanned in time to record the oscillations

on the Doppler observations but this method do not depend on the probability or luck of catching eclipses. It only needs a correct sampling of the RV signal and enough precision. So, long-period planets are more accessible than in the transit technique. Each exoplanet produce its disturbance over the star and the final result is the overlapping of all of these. Then, modelling tools look for the optimized values of the planetary model which best explains the data.

But there are some phenomena that can produce false positives too. The rotation of the star, stellar activity or starspots can introduce a Doppler effect signature and modify the received spectrum in a similar way as an exoplanet do. These effects are also in the RV as oscillations all mixed. So, all the periodicities present in the Doppler data are not produced by exoplanets.

The main value, in terms of characterization, that can be obtained from the RV data is the semi-amplitude K. It can be related to other stellar and planetary parameters, assuming $M_\star \gg M_p$, linking the semi-amplitude and the planet mass as follows:

$$K = \left(\frac{2\pi G}{P M_\star^2}\right)^{1/3} \frac{M_p \sin i}{(1-e^2)^{1/2}} \tag{4}$$

$$K \simeq 28.4 m/s \left(\frac{P}{1yr}\right)^{-1/3} \left(\frac{M_p \sin i}{M_J}\right) \left(\frac{M_\star}{M_\odot}\right)^{-2/3} \frac{1}{(1-e^2)^{1/2}} \tag{5}$$

It is not actually with M_p but the $M_p \sin i$. The problem is that RV method can not establish the orbital inclination i, which is set by the transiting method. Without photometric observations, K only gives the minimum mass of the exoplanet, if $M_\star$ is already known.

As shown, the transit and RV methods are complementary and required for a full planet characterization.

2 Objectives

The principal aim of this work is confirmation and characterization of TESS transiting candidates using photometric and archival radial velocities data. The transiting photometry method is used by TESS to discover new exoplanets, RV observations by high accuracy and stable spectrographs will confirm their presence and both data will provide the physical properties of the planet.

In its first year, TESS found many exoplanets in the southern ecliptic hemisphere and now is pointing at the northern. This work is based on discovering and validating the planet candidates combining photometry and RV data. The followed methodology in this work joints the newest and the oldest data in exoplanet research. TESS provides each month the latest and most accurate light curves for uncountable stars, where is searched the signature of a planet passing by in. These stars are cross matched with archival RV measurements that have been carried out since the late 90s by different spectrographs. This work proves the importance both of making new and accurate observations and of using those publicly-available.

Photometric and Doppler data are required to calculate the planet density. If the mass is measured, with the radius and all the other physical parameters we can classify the more than 4 000 exoplanet discovered. A better understanding of the planets in our Galaxy is the only way to be able to detect one day the second known inhabited planet.

3 Methodology

In this section, I will describe the recipe that I followed to process, search, find and confirm exoplanets in TESS photometry. The zero step of this work was the compilation of publicly-available RVs. Once the RV database was created, the procedure to follow in each sector was similar. From all the stars in my database, I choose only the ones observed in the concerned sector. This reduce the set of stars to less than two hundred. Then, I compute the RV periodogram for the selected ones. This procedure allows me to identify which stars have significant signals, that is which ones are more likely to have exoplanets, before having the photometric data. When the Full Frame Images (FFI) from TESS are available, I start to extract the light curves for the chosen stars, my sector stars, and I look for transits in them by visual inspection in the searching algorithm results. When I detect a potential transit, I check if there is a correspondence with the RV periodogram's peaks. When both methods detect an event with the same period, a new exoplanet has been discovered!

3.1 Radial velocity database

In each sector, TESS observes at a cadence of 2 minutes thousands of stars but there are not RV observations for all of them. The number of stars with enough RV data limit the number of targets of this study. First thing to do is a RV compilation of all the publicly-available measurements done by internal precise and long-term stable spectrographs. For this work, I compiled data from HIRES, HARPS and HARPS-N.

The High Resolution Echelle Spectrometer or HIRES (Vogt et al. 1994) is a grating cross-dispersed echelle spectrograph permanently located at the Nasmyth platform on one of Keck 10-m telescopes in W. M. Keck Observatory in Hawaii. It observes in the visible band between 0.3 and 1.1 microns and it has a spectral resolution between 25 000 up to 85 000. HIRES has been used to monitor F, G, K and M dwarfs stars searching for exoplanets. In 2017, the HIRES team released a catalog of observations made between 1996 and 2014. All these data were reanalyzed and corrected from systematic errors to improve accuracy and were published in Lev Tal-Or et al. 2018. It is available in VizieR (L. Tal-Or et al. 2018) and has a total of 63 169 RVs of 1 660 stars.

The High Accuracy Radial velocity Planet Searcher or HARPS (Pepe et al. 2000) is a cross-dispersed echelle spectrograph and is fiber-fed by the Cassegrain focus of ESO's 3.6m telescope in La Silla Observatory in Chile. It is located in the coudé west room of the telescope building. This allows to keep the entire instrument in an isolated, invariant and controlled environment in order to get the accuracy and long-term stability required. Thanks to this, the RV precision is down to 1m/s. HARPS main scientific goal is the search for exoplanets via RV observations. It observes in the visible band between 378nm and 691nm and it has a spectral resolution of 120 000. As in Lev Tal-Or et al. 2018, Trifonov et al. 2020 did a reanalysis of public HARPS' RVs using Spectrum Radial Velocity Analyser (SERVAL; Zechmeister, Reiners, et al. 2018) and his results are downloadable in `http://www.mpia.de/homes/trifonov/HARPS_RVBank.html`. It is a total of 205 938 RVs of 2 921 stars.

The High Accuracy Radial velocity Planet Searcher for the Northern hemisphere or HARPS-N is a high-resolution echelle spectrograph which is a clone of the original HARPS at La Silla

3.6m telescope. HARPS-N is fiber-fed by the Nasmyth B focus of the 3.6m *Telescopio Nazionale Galileo* (TNG) telescope in Roque de los Muchachos Observatory in La Palma and it is inside an isolated room in the telescope building too. Its instrumental specifications are identical to HARPS with a spectral resolution of 115 000. The observations done by HARPS-N/TNG can be queried and downloaded from the Italian Centre for Astronomical Archive website (`http://archives.ia2.inaf.it/tng/faces/search.xhtml`). Some HARPS-N observations have ownership time so, I only could download the public ones. It was a total of 26 026 RVs of 1 094 stars.

As a result, my database is a compilation of 295 133 RVs from HIRES, HARPS and HARPS-N containing 4 811 different stars (some details are summarized in Table 1).

Table 1: Specifications of the radial velocity database. *Different stars.

Instrument	Number of RV	Number of stars	Hemisphere
HIRES	63 169	1 660	Northern
HARPS	205 938	2 921	Southern
HARPS-N	26 026	1 094	Northern
Total	295 133	4 811*	

To validate and characterize the possible exoplanets, the light curve and RV measures are needed. As I explained, the limitation comes from the number of stars observed by a high-resolution spectrograph. So, it is necessary to know which stars, from my database, are going to be observed and when. The TESS mission labeled the stars with two different identifying numbers. One is the Candidate Target List (CTL) identifier which is only for the stars that are observed in 2min cadence. The other one is the TESS Input Catalog identifier (TIC or TIC ID) which includes all the stars in TESS' field of view regardless of cadence and it is the common identifier in the TESS mission. To get them for the stars in my database, I queried by coordinates in the Mikulsky Archive for Space Telescopes (MAST) Portal (`https://mast.stsci.edu/portal/Mashup/Clients/Mast/Portal.html`). The TIC ID obtained are from TESS Input Catalog Version 8 (Stassun et al. 2018). Once the TIC of each star was assigned, I used them to know in which sectors they will be observed via the Web TESS Viewing Tool (WTV; `https://heasarc.gsfc.nasa.gov/cgi-bin/tess/webtess/wtv.py`). The output from WTV is a matrix with one line per star and one column per sector. Each matrix coordinate (*star*, *sector*) has five possible values: 0, 1, 2, 3 or 4. If a star is not observed in a sector, a 0 appears in that position. Otherwise, the number of the TESS' camera that will observe the star appears. It is from this matrix that I easily get the list of observed stars in each sector.

3.2 Before sector data release

TESS observes each sector for 27 days and sends data to Earth where is hosted by MAST (`https://archive.stsci.edu/tess/`). MAST reduce, archive and make the data available to the scientific community and everybody can check them. Due to it is a very competitive field, I study the listed stars, my sector targets, before TESS data release. The list comes from the corresponding column of my data set matrix. The number of analysed targets in each sector can be consult in Table 2.

Many stars will be observed more than once because Sectors overlap. If transits are not detected the first time, it does not mean anything, and the star has to be considered in the following sectors.

As I explained, the probabilities are not big enough to miss any chance. Perhaps the planet has a period larger than 27 days or the transit fell into the gap between observations or during a TESS malfunction.

Table 2: Statistics about the observed sectors.

Sector	Different stars[a]	HIRES	HARPS	HARPS-N	new TOIs			Other planets[d]
					Total	PC[b]	KP[c]	
S17	163 (65)	114	8	59	85	78 (0)	7 (5)	8
S18	176 (81)	106	0	77	91	88 (**1**)	3 (1)	14
S19	125 (68)	85	0	48	34	31 (0)	3 (1)	3
S20	121 (55)	95	0	33	64	59 (**1**)	5 (3)	9
S21	134 (64)	92	2	48	25	19 (0)	6 (4)	8
S22	170 (72)	110	12	62	41	36 (0)	5 (4)	9
S23	183 (92)	107	35	64	52	45 (**1**)	7 (4)	10
Total	1 072	709	57	391	392	356 (**3**)	36	61

Notes. [a]In brackets, number of stars with $\geqslant$14 RV data in my sector list. [b]In brackets, number of *Planetary Candidates* in the RV database. [c]In brackets, number of *Known Planets* in the RV database. [d]Number of stars with already published planets in the RV database.

The number of listed stars from my database changes between 120 up to 180, the exact number can be consulted in Table 2, in the second column. But these total numbers include stars regardless of the number of observations, which may be insufficient to compute a useful periodogram. When the stars with 14 or more RV points are considered, this number is less than one hundred in each sector. This cutoff is not only to give a more realistic number of possible targets, but also to be able to estimate the mass. With less than ∼14 RVs not only the periodogram is useless, but possibly also the mass determination will not be possible.

The sum of the observed stars with HIRES, HARPS and HARPS-N is greater than the total because some stars were observed by more than one spectrograph. HARPS is the instrument with more measurements and stars but is the one with less listed stars, there are even sectors without. This is because sectors studied in this work are from the northern ecliptic hemisphere and HARPS is in the southern hemisphere. The instrument with more contributions is HIRES. It makes sense because HIRES is a northern spectrograph and have more stars and RV than HARPS-N. Fortunately, about ten stars are repeated and planets are searched in more than one hundred stars in each sector.

The RV analysis starts by looking for periodic signals in the data of the sectors stars. This is done with the algorithm provided by Zechmeister and Kürster 2009 which is a generalization of the Lomb-Scargle periodogram. There is a Python script (`https://github.com/mzechmeister/GLS`) in which I made some modifications of my convenience. The Lomb-Scarge periodogram is equivalent to a least-squared fit using sine waves but with modifications to analyse unequally-spaced data with presence of noise, as RV measuments are. The generalised Lomb-Scargle periodogram (GLS) presents an analytic solution to the minimization problem and some improvements such as adding an offset to the fitting formula and taking into account the measurements errors. The used fitting formula is a full sine function including an offset, $y = a\cos(\omega t) + b\sin(\omega t) + c$ where $\omega = 2\pi/P$. I used the ZK normalization for the GLS power, which maximum is 1. The GLS does

not calculate the significance of a single peak but the significance of one peak in comparison to the peaks at the other considered frequencies. For this, the false alarm probability (FAP) depends on the range of analysed frequencies and the number of independent frequencies and indicates the probability that a peak is not due to a physical phenomena. A FAP level of $X\%$ marks the power level that a peak with same power has the $X\%$ probability of being a false alarm. If the peak is greater, the FAP is smaller and vice versa. The GLS is used to search for signals in the RV data as the footprints of exoplanets and calculate the FAP of these peaks.

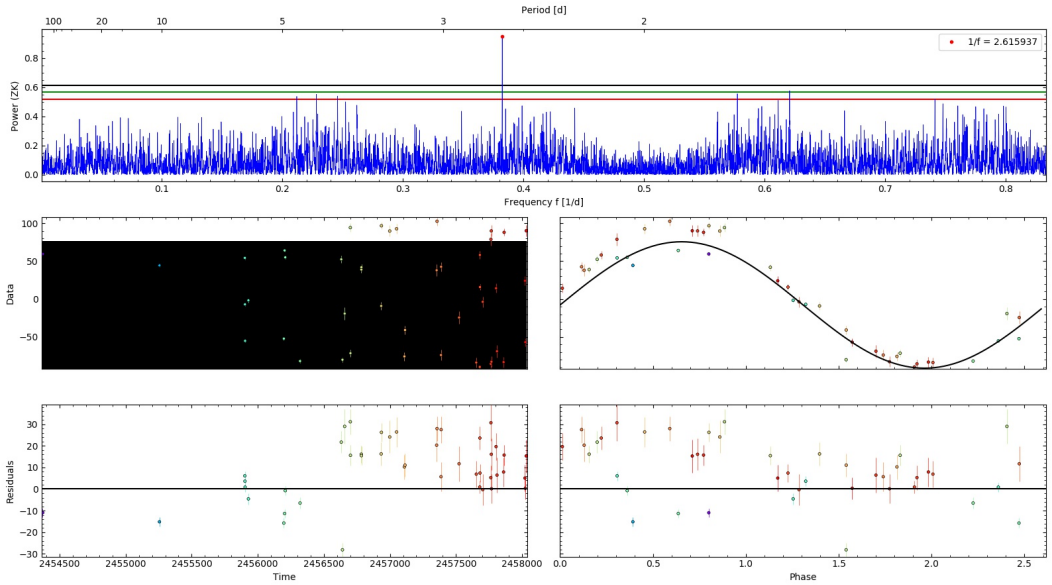

Figure 1: GLS output example of the RV analysis for TIC 356473034 (TOI 1720). *Top*: Generalised Lomb-Scargle periodogram of the RV data, in which the most significant signal is marked. It corresponds to XO-2 N b planet (P=2.616d). *Bottom left*: RV data (colored dots) along with the fitted model. *Bottom right*: Phase-folded RV data over the most significant period.

An example of the result of this process is shown in Fig. 1. It only takes few minutes to inspect all the GLS plots of the sector targets searching for significant peaks in them. When I see a periodogram with a significant peak, like Fig. 1, the first thing I do is verify if it has already discovered exoplanets, as it was in this case. Due to TESS will observe all the sky, this includes areas already observed by other missions. First query is made using the TIC ID in the The Exoplanet Follow-up Observing Program for TESS (ExoFOP-TESS; `https://exofop.ipac.caltech.edu/tess/`). This website displays many information about TIC stars: other names and identifiers, coordinates, properties, magnitudes or if it has confirmed exoplanets. Also, a quick research in the Astrophysics Data System (ADS; `https://ui.adsabs.harvard.edu/classic-form`) is done. With this search in the available bibliography it is easy to solve if a star have published planets or not.

The objectives of this RV pre-analysis are two. On one hand, identify the stars with already known planets; on the other hand, identify the stars with significant peaks in the GLS but without known planets. But this study is not infallible, it is a standard process applied systematically over all the targets and some ones can go unnoticed. The main analysis is the photometric one. At this point, all that remains is wait for the TESS data release.

3.3 *TESS* photometric data

Each sector is observed during two orbits of TESS around the Earth, that is about 27 days. Then, the images are transmitted to Earth to its processing center. The likely date to start the sector ingest to MAST Archive's servers, where TESS data are saved, is notified on their website (`https://outerspace.stsci.edu/display/TESS/TESS+Holdings+Available+by+MAST+Service`). About one day after the beginning, all these data have been archived and is available publicly in MAST Portal. MAST offers different online services to consult them. The one used in this work, via Python libraries, is the TESScut service (`https://mast.stsci.edu/tesscut/`). This service makes a cutout of FFI time series for a region of the sky. In my case, an area centered on every target star.

The light curves are extracted using the Python `tesseract` (`https://github.com/astrofelipe/tesseract`) package with some modifications of my convenience for the next steps. The output is a text file for each star with time, flux and flux error columns. But these are raw light curves, they are aperture photometric measurements extracted directly from TESS' FFI. They present smooth and abrupt variations produced by instrumental noise, systematics and random malfunctions. Also, when cameras are turned on or off there is an oscillating time before they stabilize and work properly. These oscillations occur at the beginning and ending of the sector and when the first orbit has been completed (the middle time of the observing period), because cameras switch off. For these, they need processing before looking for evidence of eclipses. I apply a mask optimized for each camera because the stabilization time will be similar for light curves that come from the same camera and then I normalize and flatten the data. Ideally, if there are not transits, the resulting light curve should be a straight line of dots around 1.

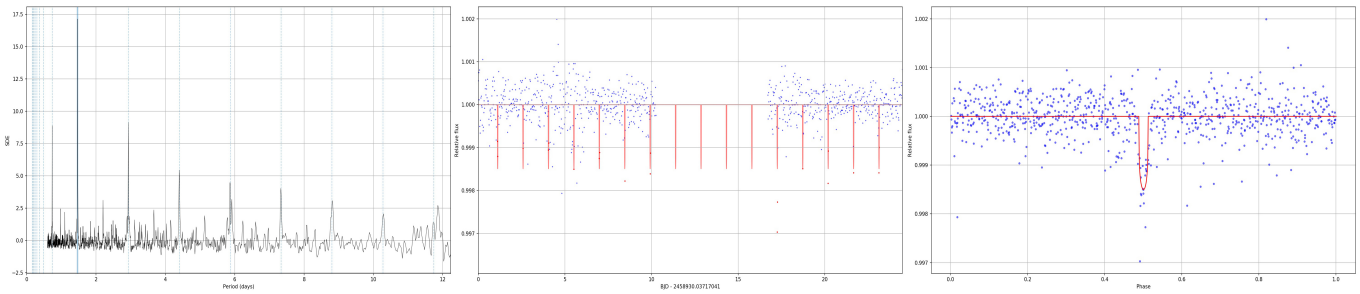

Figure 2: `TLS` output example for the analysis of TIC 390651662 (TOI 1827). *Left*: Light curve's periodogram where the significant peak and its harmonics are marked. *Middle*: 30-min cadence photometry (blue dots) along with the transiting model (red line). *Right*: Phase-folded light curve and transit model over the best period found.

I use `Transit Least Squares` algorithm (`TLS`; `https://github.com/hippke/tls`) to search for transits in the light curves. It is again a standard process over all the sector targets and its outputs are three graphics. An example of them is shown in Fig. 2. The first one is a periodogram of the photometric data. The biggest peak is the 'best' period which is the used one in the model and is supposed to be the period of the transiting planet. Even if there are not transits the program will adopt a 'best' period. The second one is a plot of the light curve with the transiting model superimposed and the last one is a plot of the light curve phase-folded.

After running the Python script over all the targets, I inspect the `TLS` plots, like the ones shown in Fig. 2, one by one. It only takes few minutes. Thanks to previous study, there are some stars that I expect to see transits in them. When I detect an unexpected transited star the procedure is similar than in the RV analysis. First, I search in the bibliography if it has known planets. Perhaps it is one of the cases without enough RVs and went unnoticed. If I do not find evidence of an already known transiting planet, the next step is a cross match with the RV data. The planet will produce oscillations in the Doppler measurements with the same periodicity of the transits.

Due to it is an automatic and unspecific process, the result is not always the best and maybe some transited stars get lost. For this, I wait for the update of the TESS Targets of Interest list. A department from MIT run their pipelines over all the stars in the FFI and then alert of the ones in which they have detected transits. These stars are the TESS Targets of Interest (TOIs). The TESS TOI Team publish that list on the TEV website (`https://tev.mit.edu/data/`) where is available to the community and alerted stars are labeled with a TOI number identifier. Some stars have already known planets and are classified as KP (*Known Planets*) TOI type. The stars without known planets but with transit-like events detected in their light curves are classified as a *Planetary Candidates* (PC).

In Table 2 there are some numbers of the alerted TOIs in the sectors analysed for this work. Total, PC or KP TOIs numbers are the new ones alerted in each sector, but because sectors overlap some can be observed more than once. The last column in Table 2 is the number of star with known planets that I found during the RV or light curve analyses. This number usually includes the KP TOIs. But the main TOIs are the ones classified as PC, the ones that have not been detected before. These are the stars classified as possible candidates and show transits events in its light curves. It is known that this kind of surveys have a lot of false positives, so the candidates need for confirmation and validation. For this, more accurate photometric observations from ground telescopes confirming the transits can be done or finding its evidence in other measurements, such as RV.

3.4 `juliet` analysis

The numbers in brackets in the column *PC* from Table 2 are the number of stars for which I have a light curve with transits and RV data. These are the potential host stars of unknown exoplanets. For these specific candidates, I realized more sophisticated analyses using `juliet`.

`juliet` (Espinoza, Kossakowski, and Brahm 2019; `https://juliet.readthedocs.io/en/latest/index.html`) is a Python algorithm that allows to compute photometric, RV and joint fit models. This code is based on other public packages for transit light curves (`batman`) and RV (`radvel`) modeling and allows to include Gaussian Processes (GPs) to explain the noise present in the data via other public tools (`george` and `celerite`). It allows for a variety of parametrizations and includes a method to perform model comparison. Instead of using Markov chain Monte Carlo (MCMC) technique, `juliet` uses a nested sampling algorithm to explore all the parameter space and also compute the Bayesian model log-evidence ($\ln Z$). That is performed using *MultiNest* via `PyMultiNest` or `dynesty` packages to compare different models. Higher values of $\ln Z$ represent higher evidences. A difference in the Bayesian log-evidence less than $\sim$2 indicates that there are not great differences and they are similar, then the simplest ones takes advantage. If a model has a $\Delta \ln Z$ greater than 5, this one is strongly favoured in front of the other.

The photometry and RV models have some common parameters such as the period P, time of transit-center t_0, the eccentricity e and the argument of periastron passage of the orbit ω. e and ω are fixed to 0 and 90º, respectively, for circular orbits. For models with eccentric orbits, I use the alternative parametrization $\mathcal{S}_1 = \sqrt{e}\sin\omega$ and $\mathcal{S}_2 = \sqrt{e}\cos\omega$, with $e = \mathcal{S}_1^2 + \mathcal{S}_2^2 \leqslant 1$. The other parameters depend on if photometry, RV or both data are fitted.

In the photometry fits, the stellar density is required and is used to obtain the semi-major axis a. Rather than fitting for the impact parameter of the orbit $b = (a/R_\star)\cos(i)$ (where i is the orbit inclination) and the planet-to-star radius ratio $p = R_p/R_\star = \sqrt{\Delta F}$, I use the parameters r_1 and r_2, suggested by `juliet`'s developer, that guarantee the full exploration of the physicals values for (b, p). These alternative parameters are sampled with uniform priors between its physical limits. The photometric instruments need some parameters to characterize them, such as the dilution factor, which is fixed to 1 if there are not evidences of nearby companions. The models include a photometric jitter term in quadrature σ_{instr} for the photometric instrument uncertainties and a relative flux offset M_{instr} for the data. Also, I will use in the photometry models a two-parameter law for the limb darkening of the star via the q_1 and q_2 parameters.

In the RV fits, the semi-amplitude K is required. For the RV instruments, as the photometric ones, a jitter term in quadrature σ_{instr} and a systemic velocity μ_{instr} are considered too.

RV and photometry data may have signals behind the planetary ones from unknown nature and difficult to fit. For this, Gaussian Processes are used as an approximation to the unknown function which explains the underlying stochastic processes. They are used when data are not purely white noise distributed. GPs are stochastic processes in which every finite set of data are multivariate normal distributed. There are different GP kernels and `juliet` have a catalog of the main ones. If the model include GP, their hyperparameters have to be defined too.

The outputs of `juliet` are the orbital model, its Bayesian log-evidence and the posterior distributions for the planetary system parameters from which the 1σ errors can be calculated.

4 Results

The methodology explained above was applied to analyse 7 sectors, from Sector 17 to 23. As it is shown in Table 2, a total of 356 new TOI planetary candidates were announced but I had RVs only for 3 stars that showed signs of a transiting planet and without known planets. They represent ∼1% of the total PC TOI, but they do not require further observations to be confirmed and validated, only making use of archival data. The results from this work are the study of these 3 candidates: TOI 1611, TOI 1718 and TOI 1827.

TOI 1611 was observed in Sectors 18, 19 and 20, TOI 1718 in Sector 20 and TOI 1827 in Sector 23. First, I will explain the results obtained for TOI 1718 and TOI 1827. Finally, I will analyse in detail the case of TOI 1611, wich is the main result of this work.

4.1 TOI 1718

HD 58727 (TIC 257241363, TOI 1718) is a high-proper motion and G5 type star with a radius of $R_\star = 0.94 \pm 0.05 R_\odot$ and a mass of $M_\star = 0.93 \pm 0.11 M_\odot$ (Stassun et al. 2018). It is at $\alpha = 7h28m4.35$, $\delta = +30º19m20.65$, in the Gemini Constellation, at a distance of 52.38 ± 0.09pc (Gaia Collaboration et al. 2018). It was observed by TESS from December, 24th 2019 until January, 21st 2020 during Sector 20. After its observations, it was announced as TOI 1718 on February, 20th 2020. The Science Processing Operations Center (SPOC) detected a signal with a period of 5.58d and $\Delta F = 1855 \pm 44$ that corresponds to a radius of about $4.0 \pm 0.5 R_\oplus$.

Unfortunately, this star is one of the cases for which there are few observations in the database. It was in my Sector 20 list because there are 3 RV points from HIRES, not enough to compute a periodogram or confirm the transit signal. Thus, I look for more RV observations. My database only includes spectrographs with publicly-available data that can be downloaded massively due to the methodology I follow. But most archive can only be queried for specific objects or coordinates, which is the actual situation. So, I look for more observations in other archives and I found 16 RV measurements in the SOPHIE spectrograph archive, but their values were very scattered and not useful to confirm the short period transiting planet.

After this search, I studied the feasibility to observe the candidate with one of the spectrographs located at the Canaries Observatories. One measurement each day during a week could be enough to sample a full period because it is of about 5 days. I used the tool STARALT (`http://catserver.ing.iac.es/staralt/index.php`) to determine when TOI 1718 was visible from Canary Islands. Due to its altitude greater than 60º at the beginning of the late February's nights, I proposed to observe the star to my TFM's tutors, who accepted. TOI 1718 was scheduled to be observed with HARPS-N at the end of February but a big dust storm affected the Canary Islands and the observations were cancelled. So, it was impossible to get Doppler effect measurements for this target before it set and its mass determination is not possible without RV data.

Because the weather, the only useful data for TOI 1718 is the photometric one. The light curve analysed with `juliet` is the 2-min integration TESS photometry extracted from the MAST archive. The priors used for P and t_0 are Gaussian distributions centered on the `TLS` results and considering a circular orbit.

The results of the fitting are shown in Figure 3 and are consistent with those provided by SPOC. Using Eq. 1 and the star radius, the value that I get for R_p is $4.04^{+0.09}_{-0.07} R_\oplus$ which is

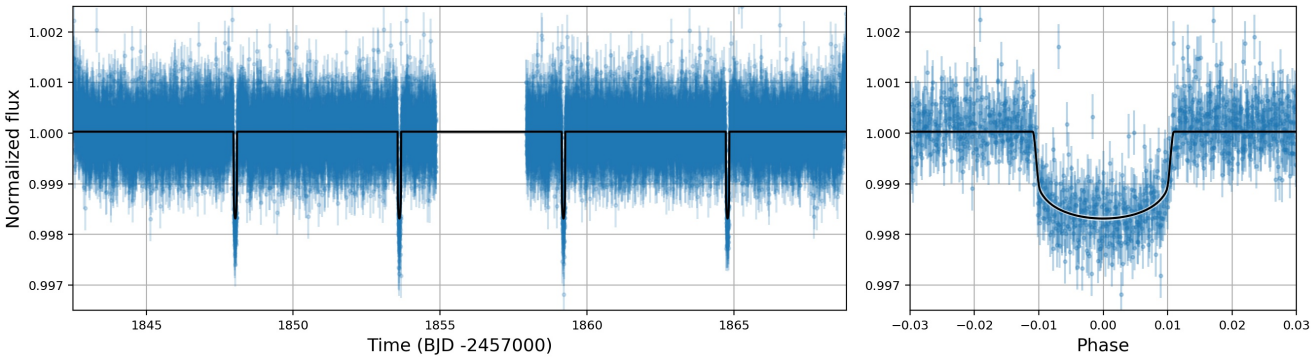

Figure 3: Results from the 2-min cadence photometry fit with `juliet` for TOI 1718. *Left*: *TESS* photometric data (blue dots with error bars) along with the best-fit transit model (solid black line). *Right*: Phase-folded light curve over the best-fit P (5.5869 ± 0.0003 d) and t_0 ($1848.0271^{+0.0005}_{-0.0006}$).

very similar to the alerted one and with errors 5 times smaller. I do not compute transit time variations because there are only 4 transits in less than 20 days and no other data to compare hypothetical variations. Also, this analysis are better with more transits and more spanned in time.

Its transit depths are similar, there are no secondary eclipses and the transits are not V-shaped. It does not seem a false positive, but the planet can not be validated neither its mass determined without further observations. The derived planetary parameters obtained from the photometry fit with `juliet` are shown in Table 5. Its equilibrium temperature T_{eq} is $1\,000^{+50}_{-21} K$, which is the theoretical planet temperature if it is treated as a black body heated by the host star. This model does not consider other effects that could modify the planetary temperature like greenhouse effect and are assuming zero Bond albedo. Insolation S is the power per unit of area received from the star in the form of radiation and it is $166^{+35}_{-14} S_{\oplus}$.

4.2 TOI 1827

GJ 486 (TIC 390651552, TOI 1827) is a high proper-motion star classified as M3.5V. It is located at 8.076pc from Earth at $\alpha = 21h40m44.78$, $\delta = +84^{o}20m00.56$ (Gaia Collaboration et al. 2018) in the Virgo Constellation, is one of the brightest M dwarfs with J=7.195mag and has a radius of $R_{\star} = 0.331 \pm 0.010 R_{\odot}$ and a mass of $M_{\star} = 0.313 \pm 0.020 M_{\odot}$ (Stassun et al. 2018). It was observed by TESS from March, 18th 2020 until April, 16th 2020 during Sector 23 and it was announced as TOI 1827 on May, 5th 2020. SPOC detected a signal with a period of ∼1.46d, a total transit time t_T of 1.01±0.15h and $\Delta F = 1600 \pm 58$ that corresponds to a planet radius of about $1.3 \pm 0.5 R_{\oplus}$.

Despite its short transit duration, the `TLS` analysis of the flattened 30-min cadence light curve found the ∼1.46 value as the best-fit period, as was shown in Fig 2. For a better performance of the `juliet` fitting, the 2-min integration photometry was extracted from MAST archive. The P and t_0 priors are normal distributions centered at `TLS` values and considering a circular orbit. The results of the photometric fitting are consistent with those published in the alert and the transit model is shown in Figure 4.

The photometric data can be used to detect non transiting planets via the transit timing variations (TTVs) of the transiting ones. The transits can be predict with a great precision in

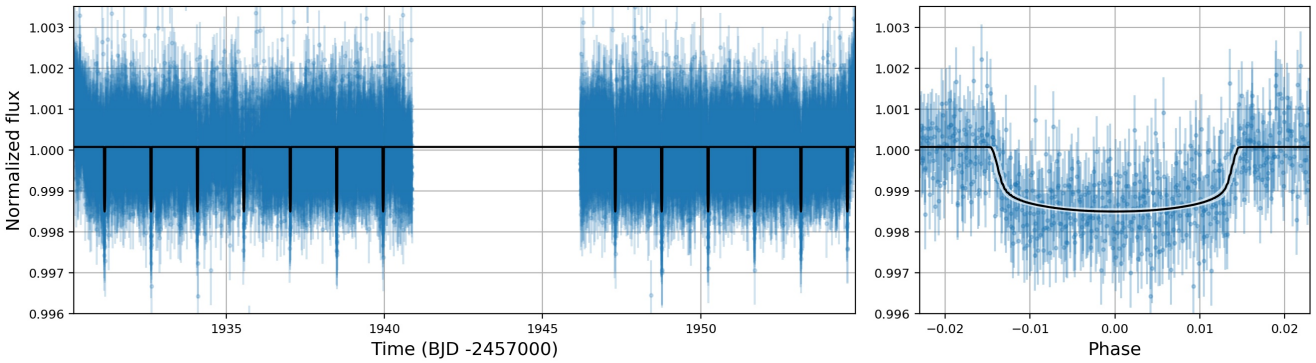

Figure 4: Results from the 2-min integration photometry fit with `juliet` for TOI 1827. *Left*: *TESS* photometric data (blue dots with error bars) along with the best-fit transit model (solid black line). *Right*: Phase-folded light curve over the best-fit P (1.46713±0.00006 d) and t_0 (1931.1593±0.0006).

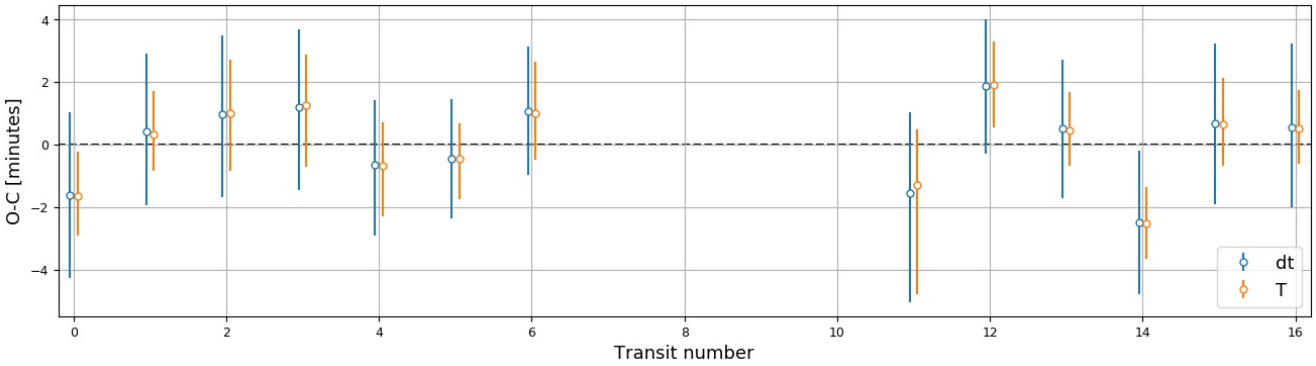

Figure 5: Results from the transit time variations (TTVs) with `juliet` for TOI 1827. Differences between the observed and calculated (O-C) time of transit. The values are slightly shifted from the transit number for a better comparison of both methods.

a Keplerian orbit, with P and t_0 well known. So, the differences between the observed and the calculated times of the eclipses (O-C) can be used to detect perturbations in the Keplerian period produced by interactions with unseen companions. I performed the two TTVs analyses allowed by `juliet`.

The first one (T method in Fig. 5), I added a time-of-transit parameter T_n for each visible transit with normal distributions. The TTVs are calculated from T_ns, P and t_0 posteriors as $TTV_n = T_n - (t_0 + nP)$. The second one (dt method in Fig. 5), a δt_n parameter is added for each transit to characterize the O-C differences using normal distributions centered at 0. These δt are already the TTV values.

The results of both methods are similar and are shown in the Figure 5. The periodogram of the TTVs shows a peak at 4.8 days with FAP> 10%, but there are not other visible transits. The TTVs error limits are consistent with the absence of a companion for TOI 1827b.

GJ 486 has a total of 74 RV observations in my database, where 12 RV points come from HARPS over ∼7 years and 62 are from HIRES over ∼16 years of observations. The first analysis

was a study of periodicities present in the data. Periodograms do not have significant signals neither peaks near 1.46d or the 4.8d period from the TTVs.

The second one was a fit with `juliet` using normal priors for P and t_0 and a uniform distribution between 0 and 10m/s for the semi-amplitude K. I also considered an exponential GP kernel due to the big error bars of data. The semi-amplitude from the RV fit is $1.2\pm0.5 m/s$.

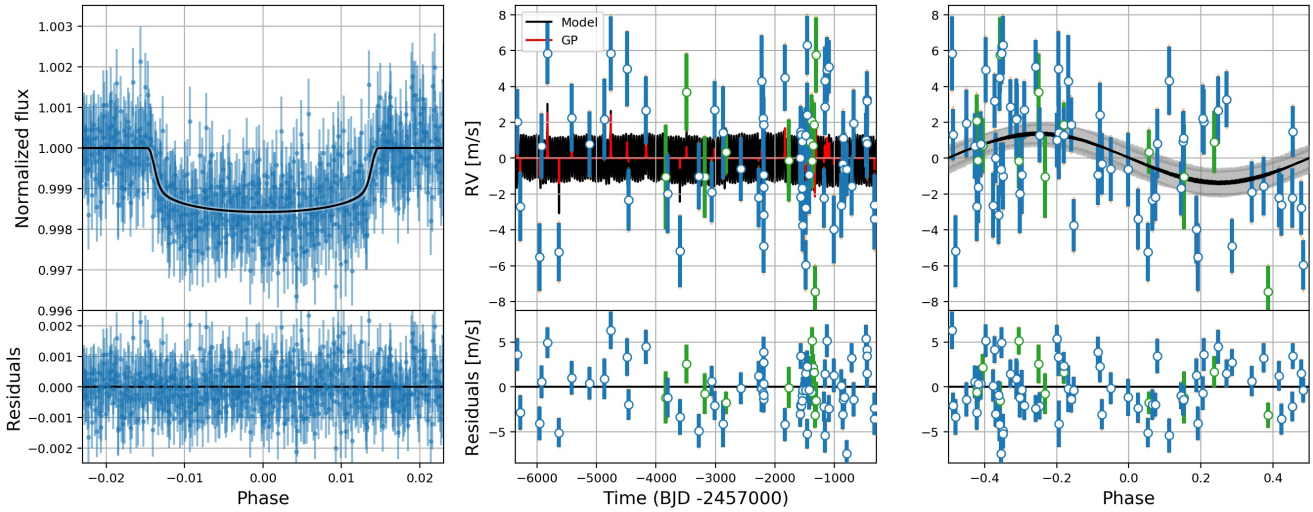

Figure 6: Results from the joint fit model with `juliet`. *Left panel*: Phase-folded TESS photometric data (blue dots with error bars) with the transiting model (solid black line). *Middle panel*: HIRES (blue dots with error bars) and HARPS (green dots with error bars) data along with the RV model (solid black line) and the GP (red line). *Right panel*: RVs and Keplerian component (solid black line with grey areas denoting the 68% CI) phase-folded to the joint fit P (1.467144±0.000023d) and t_0 (1931.1592±0.0004).

After analysing the RV and photometry data separately, I performed a joint fit using the same priors as in the previous separate models and an exponential GP kernel to explain the correlated noise in the RVs. The determination of the RV parameters have improved from the RV-only fit and the semi-amplitude has increased to $1.5\pm0.5 m/s$ but it is still in the 68% credibility intervals (CI) of the RV-only posterior. The derived transit parameters have not changed significantly from the photometry-only fit, even uncertainties have been reduced.

Considering the results of the joint model, the derived planetary parameters obtained for TOI 1827b are shown in Table 5. The parameters obtained from the light curve are consistent with the published ones by SPOC but with better uncertainties. The radius obtained is $1.39^{+0.06}_{-0.05} R_\oplus$ with errors 10 times smaller. Although the RVs are spread over years, the short period is well sampled. Due to RVs data precision, the planetary mass is $1.2\pm0.4 M_\oplus$. More data with higher time cadence is needed to improve the mass detection and reduce its uncertainty.

Also, this star was observed by CARMENES, a spectrograph at Observatorio de Calar Alto that searches for exoplanets around M dwarfs. The CARMENES survey had private RV data and were able to refine my mass determination independently. Their results are going to be published soon (*Trifonov et al., in prep.*).

5 TOI 1611

In this chapter, I focus on HD 207897 (TIC 264678534, TOI 1611), a bright (V=8.37mag, K=6.31mag) nearby ($d = 28.32 \pm 0.03$pc) K0 type and high-proper motion star with a radius of $R_\star = 0.78 \pm 0.05 R_\odot$ and a mass of $M_\star = 0.85 \pm 0.11 M_\odot$ (Stassun et al. 2018). It is a circumpolar star, near Polaris, in the Cepheus Constellation ($\alpha = 21h40m44.78$, $\delta = +84°20m00.56$; Gaia Collaboration et al. 2018). It was observed by TESS in 2-min short-cadence integrations from November, 2nd 2019 until January, 21st 2020 during Sectors 18, 19 and 20 and is going to be observed again in Sectors 25 and 26 from May, 13th 2020 to July, 4th 2020. After its observations on Sector 18, it was announced as TOI 1611 on December, 20th 2019. SPOC detected a signal with a period of 16.19d and $\Delta F = 990 \pm 3$ that corresponds to a radius of about $2.70 \pm 0.25 R_\oplus$.

Table 3: Stellar parameters of TOI 1611.

Identifier	Value	Source	**Parameter**	Value	Source
HD ID	207897	HD	R.A. (h:m:s)	21:40:44.78	Gaia
TIC ID	264678534	TESS	Dec (d:m:s)	+84:20:00.56	Gaia
TOI ID	1611	TOI Alert	Parallax (mas)	35.31 ± 0.04	Gaia
Gaia ID	2300641567596591488	Gaia	Distance (pc)	28.32 ± 0.03	Gaia
2MASS ID	J21404490+8420005	2MASS	Spectral Type	K0	(1)
Properties	Value	Source	**Magnitudes**	Value	Source
$M_\star$ ($M_\odot$)	0.85 ± 0.11	TESS	T (mag)	7.583 ±0.006	TESS
$R_\star$ ($R_\odot$)	$0.79^{+0.01}_{-0.04}$	Gaia	G (mag)	8.1304 ±0.0004	Gaia
$L_\star$ ($L_\odot$)	$0.365^{+0.00}_{-0.01}$	Gaia	B (mag)	9.264 ± 0.026	TESS
T_{eff} (K)	5052^{+115}_{-42}	Gaia	V (mag)	8.37 ± 0.03	TESS
log g	4.58 ± 0.09	TESS	J (mag)	6.830 ± 0.023	2MASS
$\log R'_{HK}$	-4.85 ± 0.02	(1), (2)	H (mag)	6.391 ± 0.034	2MASS
Age (Gyr)	4.05	(2)	K (mag)	6.312 ± 0.026	2MASS

References. HD: Cannon and Pickering 1993; TESS: Stassun et al. 2018; Gaia: Gaia Collaboration et al. 2018; 2MASS: Cutri et al. 2003; (1) Boro Saikia et al. 2018; (2) Isaacson and Fischer 2010

TOI 1611 was in my target list because I had 6 RV points from HIRES, but with large error bars and too spread in time. So, I look for more RV observations like in the TOI 1718 analysis. In this case, I found useful observations in the SOPHIE archive (`http://atlas.obs-hp.fr/sophie/index.html`), the on-line database of high-resolution spectra and RV taken with SOPHIE.

SOPHIE is a cross-dispersed échelle spectrograph installed at the 1.93m telescope in Haute-Provence Observatory (OHP) in France. It observes in the visible band in the range between 387.2-694.3nm and its High Resolution mode has a spectral resolution of 75 000. In the SOPHIE archive there were 44 RV points and their periodogram showed a significant peak at 16.19d, consistent with the transit period. New observations with SOPHIE were done in collaboration with Neda Heidari, a doctoral student from *Laboratoire d'Astrophysique de Marseille* (LAM), who also reported its discovery. I will use only the SOPHIE data due to the difference of quality between SOPHIE and HIRES observations, SOPHIE's errors are smaller. Also, my analyses for this planet are being written in an article in collaboration with the LAM group.

5.1 *TESS* photometric analysis

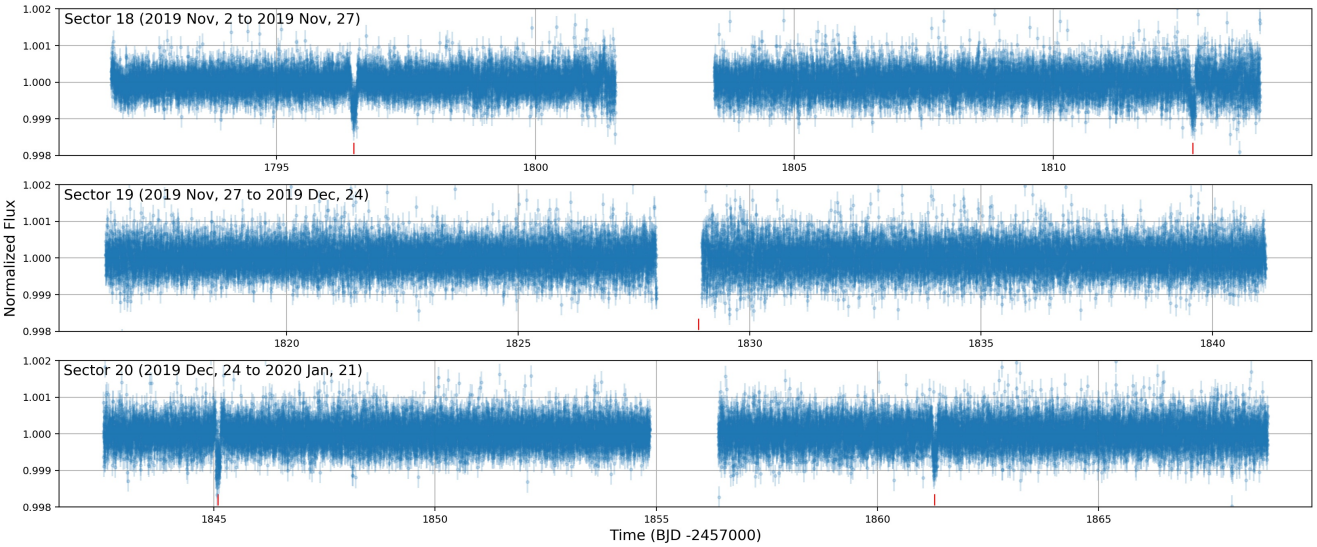

Figure 7: The full *TESS* light curve (blue points with errors) on the 2-minutes exposures from Sectors 18, 19 and 20. Time transits for TOI 1611b are marked in red.

The TESS spacecraft observed TOI 1718 during three consecutive sectors from November 2, 2019 to January 21, 2020 using Camera 3. The photometric observations at short cadence are shown in Fig. 7. After the Sector 18 observations, it was alerted as a planetary candidate detecting two transits separated from each other by ∼16.2d. Post stamps images from FFI and survey images from the Two Micron All-Sky Survey (2MASS) and the Digitized Sky Survey (DSS) show that HD 207897 have near visual companions in the field. Due to TESS has a large pixel size of 21", it is very important the properly determination of close-by targets affectation into the light curve, even if the transit events are really from a centered target. The binary system configuration was rejected because the symmetry between odd and even eclipses and its transits' shape. Precise photometric observations or high angular resolution images were not necessary because the RV data of HD 207897 showed a signal in the GLS consistent with the detected period.

The light curve used in the `juliet` analyses are the 2-min cadence photometry (see Fig. 7) which was flattened by Diego Hidalgo as in Hidalgo et al. 2020. In Sector 19, no transit was observed because it fell into the data downlink gap, so only 4 transits were catch.

The priors for P and t_0 introduced in `juliet` are normal distributions centered on the values from `TLS`. The eccentricity e and the argument of periastron passage of the orbit ω are fixed to 0 and 90°, respectively. The TESS dilution factor D_{TESS} was fixed to 1 for simplicity and to save computational time but it should be taken into account for more accurate analyses due to the nearby companions. A photometric jitter σ_{TESS} for TESS data were added in the model and I used a quadratic limb darkening law.

The results of the `juliet` photometric fitting are consistent with those provided by SPOC and `TLS` transit search, but with better uncertainties. The transit fit and the phase-folded data are shown in Fig. 8. I explored the possibility of another transiting planet adding it to the model but the fit did not show that evidence and also the $\ln Z$ did not favor it.

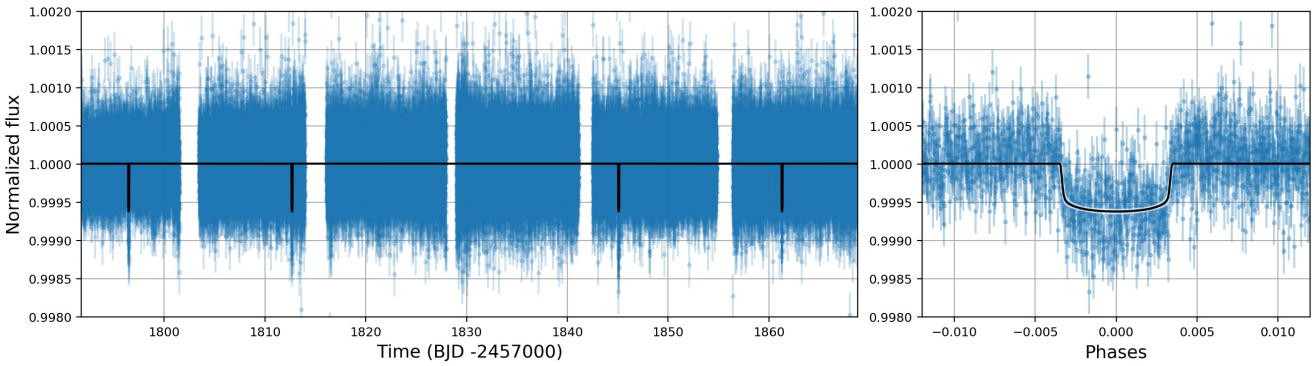

Figure 8: Results from the photometric fit with `juliet`. *Left: TESS* photometric data (blue dots with error bars) along with the best-fit transit model (solid black line). *Right:* Phase-folded light curve over the best-fit P (16.2009 ± 0.0006d) and t_0 (1796.4951 ± 0.0013).

As in the TOI 1827 case, I performed two TTVs analyses. Because transits are spanned in more than 60 days, they can help to find long-term trend variations. Because transit number 2 (numbering the first one with $n = 0$) fell into a gap between data, there are O-C for n= 0, 1, 3 and 4.

From the first method, the variations are calculated as $\mathrm{TTV}_n = T_n - (t_0 + nP)$. The O-C for the four transits are $\mathrm{TTV}_0 = 0.1min$, $\mathrm{TTV}_1 = 0.2min$, $\mathrm{TTV}_3 = -0.1min$ and $\mathrm{TTV}_4 = 0.1min$ and their uncertainties are about $\pm$5 minutes. From the second one, the δt_n output posteriors are $\delta t_0 = -0.1min$, $\delta t_1 = 0.2min$, $\delta t_3 = -0.1min$ and $\delta t_4 = -0.04min$ also with uncertainties of $\pm$5 minutes. The computed TTVs are positive and negative without a pattern and are very near to 0. The errors limits of $\pm$5 minutes represent a very small variation in the total duration of the transit t_T, which is of $\sim$3h. Also the models including TTVs are indistinguishable from the one without. It should be note that the TTV method improves when more eclipses are observed. Four eclipses are not sufficient for solid conclusions but the results from both analyses are consistent with the absence of perturbations over the orbit of TOI 1611b.

5.2 Radial velocity analysis

In the SOPHIE archive there were 44 radial velocities measurements and their GLS presented a very significant peak near 16.2d. These spectra were taken between July 8, 2012 and September 18, 2015. Due to the collaboration with the SOPHIE team, we obtained 23 new observations with SOPHIE between January 13, 2020 and February 23, 2020. In total, 67 observations with SOPHIE spectrograph are used in this work. The RV's values were extracted directly from spectra using SERVAL (Zechmeister, Reiners, et al. 2018). SERVAL code is based on a least-squared algorithm instead of a cross-correlation function (CCF) method. To obtain the values, each spectrum is fitted to a high signal-to-noise template build from all the spectra to compute the relative radial velocities with respect to the template. The periodogram calculated with the 67 measurements is shown in Fig. 9*a*. Grey horizontal lines in the GLS indicate the theoretical 10%, 1% and 0.1% FAP levels, respectively from bottom to top, calculated as described in Zechmeister and Kürster 2009. The most prominent and significant peaks in the RV data are at 15.75, 16.19, $\sim$27 and $\sim$35 days. Also, there are long-term trends with false-alarm probabilities $< 1\%$ which biggest peak is

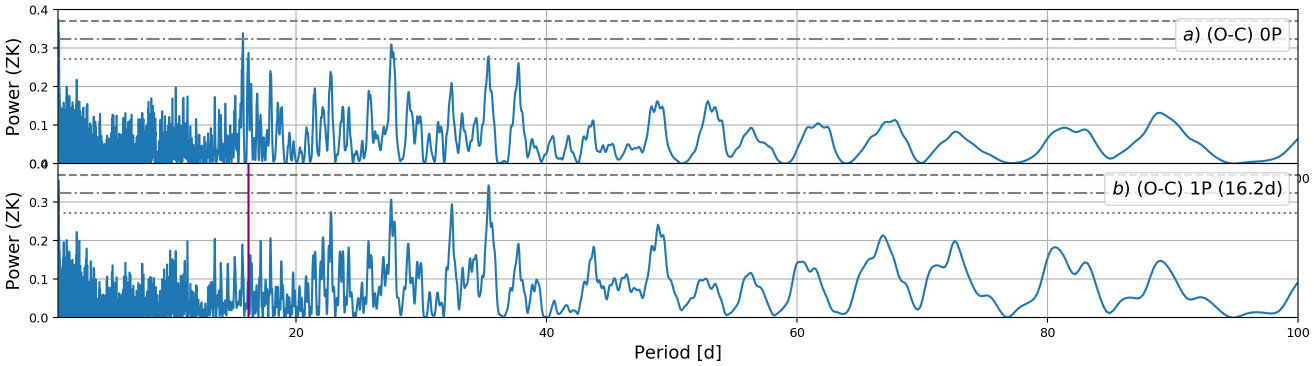

Figure 9: Comparative between periodograms for the RV data (a) and the residuals from the 1-planet model `juliet` fitting (b). Grey horizontal lines indicate the theoretical 10% (dotted), 1% (dash-dotted) and 0.1% (dashed) false-alarm probability (FAP) levels. Color vertical line indicates the planet period subtracted

at ∼143d.

As in the photometric analyses, I use `juliet` to perform different models. The first analysis is based on the transits results. The introduced priors for P, t_0, e and ω are the same as in the photometric case. For the semi-amplitude K, a uniform distribution between 0 and 20 m/s is used. Also, a jitter term σ_{SOPHIE} and an offset μ_{SOPHIE} for the SOPHIE data are considered in all the RV fits.

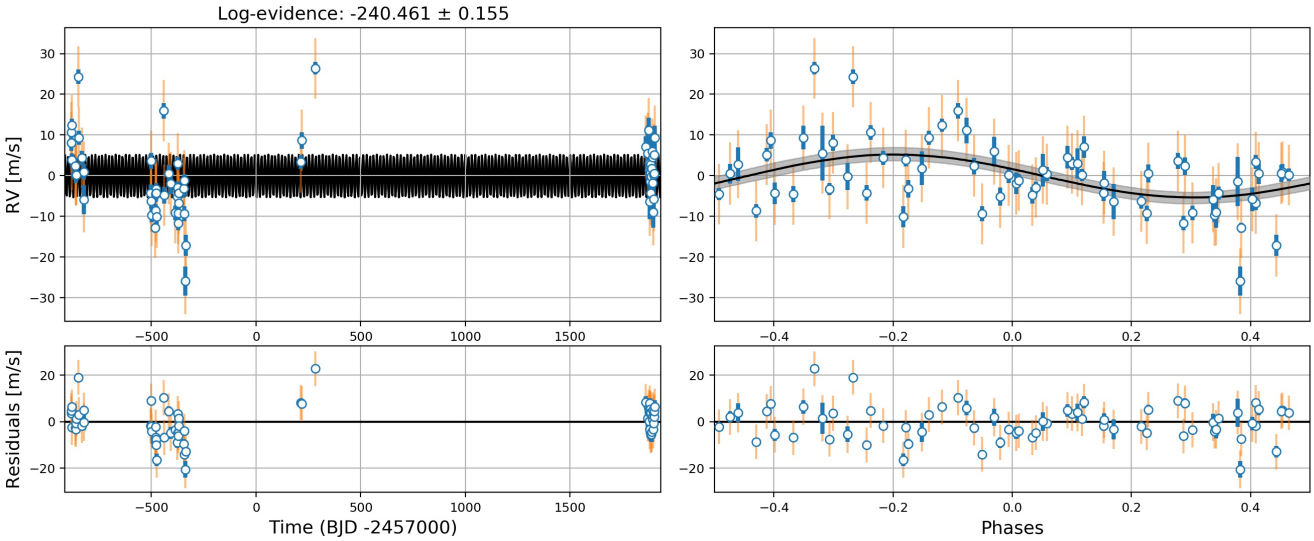

Figure 10: Results from the RV fit of 1-planet model with `juliet`. *Left panel*: SOPHIE RV data (blue dots with blue error bars) along with the RV model (solid black line). *Right panel*: RVs and Keplerian component (solid black line with grey areas denoting the 68% CI) phase-folded to best-fit P ($16.203^{+0.006}_{-0.007}$d) and t_0 ($1796.47^{+0.10}_{-0.08}$). Orange error bars include the jitter.

The model of the keplerian orbit of the 16.2d period is shown in Fig. 10 and the GLS of this model residuals are shown in Fig. 9*b*. The full period has been correctly sampled with data spread

along the four quadrants but it is not a perfect adjustment because the residuals are far from 0. The residuals do not look like white noise centered around 0, but it seems to have a structure. The P and t_0 posteriors are consistent with the values obtained from TESS photometry. The semi-amplitude posterior of this 16.2d-period model is $K \simeq 5 \pm 1$ m/s.

Furthermore, the periodogram of the residuals (Fig. 9*b*) no longer shows the 15.7d peak. That could be because it was an alias of the planet signal. It was close to the 1-year alias of 16.2d which is 15.51d, or because it was near the planetary peak itself. Now, the most prominent peaks are at 35d, 27d and 32d, in that order. The 27d signal has kept its power but the thirties one has increased.

The difficulty is to identify the cause of these signals. TESS data confirm that the 16.2d period is produced by a planet but there are not other variations in the photometry. We do not know if the other signals are produced by non-transiting planets or stellar activity. The distinction between planetary and activity modulations in the RV time-series is that fist one is always present. Stars have epochs of more or less activity but planets are always revolving. Taking advantage of this, there are some analyses that can be done.

5.2.1 Powergram analysis

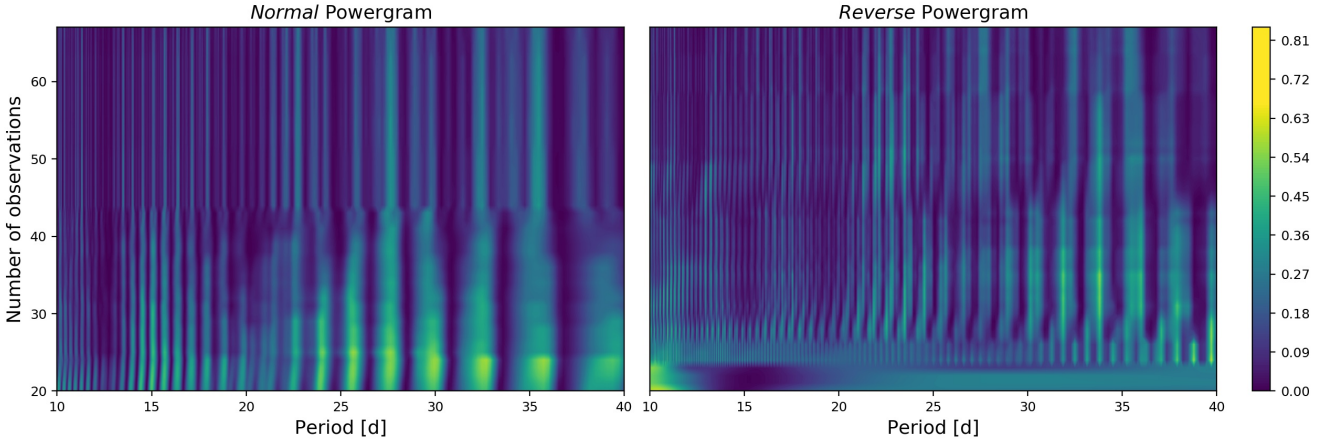

Figure 11: *Normal* (left) and *reverse* (right) powergrams centred on the period of interest computed using the residuals from 16.2d-period model (Fig. 10). Lateral color bar indicates the normalized ZK power scale.

In order to study the origin of the unknown peaks detected, many GLS are computed using different number of data points. The data used are the residuals from the `juliet` model which no more present effects produced by the transiting planet.

Due to the number of available observations, a GLS with half of the residuals can be computed, then another GLS by adding the following point and so on until all the data are used. These GLS can be displayed as a powergram (a spectrogram of the power) of the residuals, using a color scale as a power indicator. In the powergram calculation, the points can be sorted in chronological or reverse order. To distinguish both cases, I call them as *normal* and *reverse*, respectively. Powergrams allow to see the evolution of the periodicities' power along the measurements, which are used as proxy of time. Therefore, a planetary effect should be visible from the beginning, with few observations, and maybe increases its significance when observations increases too or it remains

constant. But activity peaks are supposed to vary their power over time without a pattern. These signals' behaviours are supposed to be present equally in both type of powergrams. The Figure 11 shows the powergrams in the range of periods of interest.

Spectral resolution depends on the base-line of data. The peaks are better definite when the observations are more spanned in time. The normal powergram starts with the archival data which was taken along 3 years and the reverse one with the new observations taken during about 40 days. For this, the spectral resolution in the normal one is grater than in the reverse one for few observations. At the end, both powergrams have used the same data and are identical. In the normal one, the peaks narrow when more observations are taken into account. Their maximums are centered from the beginning at the periods of interest, 27, 32 and 35 days. In the reversed, when some points from archive are added the resolution suddenly increase but the main periods are not so clear as in the normal powergram. The most prominent is the 35d one, the only one visible from start to finish. There is a peak at ∼34d that disappears when the 32d one increases. Some periods present slightly displacements of its maximum and also splittings when the spectral resolution increases. But the only appreciable effect is the narrowing of the peaks and a little power decrease.

The powergrams of the RV data do not allow to discard any hypothesis about the nature of these periods and only confirm the signals present in the GLS from the RV data and residuals.

5.2.2 Semi-amplitude analysis

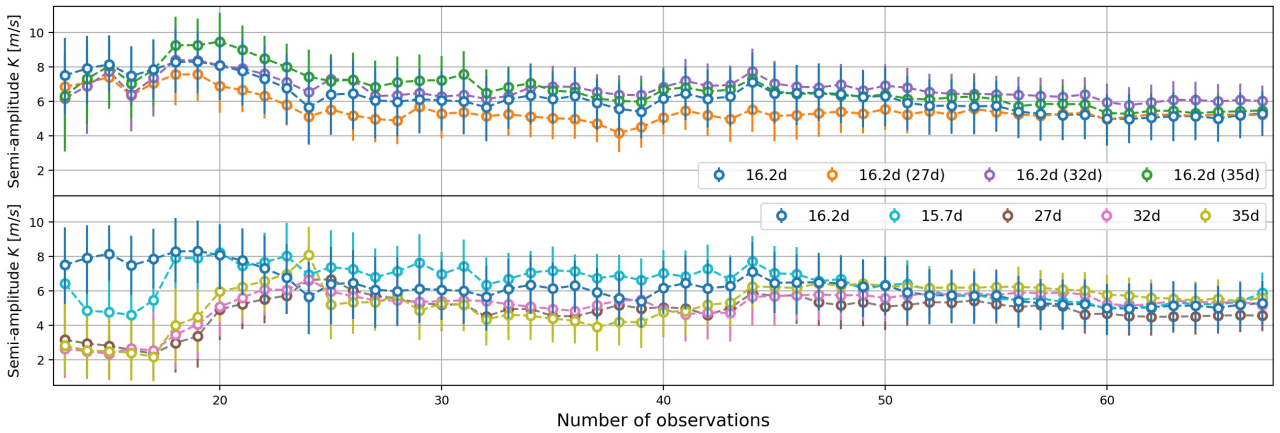

Figure 12: Comparative evolution of the signals' semi-amplitude modeled varying the number of observations to fit with `juliet`. Error bars denote the 68% posterior credibility intervals (CI). *Top:* Ks of the transiting planet from the single (blue points) and multi-planet models. *Bottom:* Ks' comparison for all the significant signals.

The idea of this analysis is similar to the previous one. Planets' perturbation will be always of the same semi-amplitude but for the stellar activity will not be due to its variability. The planet K value will be similar over time and the one for stellar activity could vary. For this, I compute the same `juliet` models with different RV data number, as I did in the normal powergram calculations. The significant signals are fitted as Keplerian circular orbits ($e = 0$ and $\omega = 90^{\text{o}}$ fixed) and the other priors are the same as in the original model. Period and t_0 priors for the signals are normal

distributions centered on the best value after some test runs with uniform priors. The single-planet models evaluate the planetary signal and the 15.7d period. The multi-planet models evaluate the transiting planet and one of the 27d, 32d or 35d signals. The Ks values for the 16.2d period from multi-planet models are used in the analysis too. The evolution of the 15.7d, 16.2d, 27d, 34d, 35d semi-amplitudes is shown in Fig. 12.

The top panel collects the 16.2d-period semi-amplitudes from the diverse models. The four Ks present comparable behaviours. They start in a high value and then decrease to the final value of ∼5m/s. With equal number of observations, the values are consistent within their error bars, even almost all the values are within the upper and lower limits.

The bottom panel shows the semi-amplitudes for the interest periods: the double peak in the original data at 15.7d and 16.2d and the significant signals in the GLS from the 16.2d-model residuals which are at 27d, 34d and 35d. The behaviour of 15.7d period at the beginning is quite different from the rest, it is not like the residuals periods or the planet signal but it approaches to the ∼5m/s at the end. The residuals periods have a parallel evolution, they start with lower values and climb until coincide with the 16.2d model.

As can be seen, the differences between semi-amplitudes are bigger before taking into account the new observations, before the 44 number of observations. After that, the curves trend to ∼5m/s and they are within their error bars. There are not random variations, only the 15d-period has a strange behaviour at the beginning. As in the powergrams analysis, there are not strong evidences to determine the origin of the signals. The great difference between the planet and the residuals period is in the archival data from 13 to 25 observations. The precision in the RV makes that the semi-amplitude error bars are of the order of its value and almost all of them are in their upper and lower error limits. Therefore, it is not a reliable method and it is insufficient to draw conclusions.

5.2.3 Activity analyses

Another way to find if there is any evidence of stellar activity in the spectra is looking at the activity indicators from the SERVAL analysis. For this, I used the chromatic RV index and the differential line width.

SERVAL algorithm compute the RV of the spectrum as a simple weighted average of each RV from the different echelle orders. Since echelle orders are related with wavelength, a lineal dependency between RV and wavelength can be obtained. The slope of the modeled straight line is what is called chromatic RV index (CRX). Due to the Doppler effect depends on wavelength, there will be a CRX≠0 and it is expected to keep its value in all the observations. The flux blocked by star spots may vary from distinct wavelengths and this will produce a change in the slope. The CRX is closely attached to the RV because is calculate with the same spectral lines. The units of CRX are m/s (the same as the RV) per wavelength unit per e (Euler's number) because the relation with the wavelength is via natural logarithm. For this, CRX is a good estimator of stellar activity in the RV measurements.

In addition, since SERVAL do not use a CCF method, they should find an analogous to the Gaussian function moments which give information about the width and the asymmetries. This is the work of the so-called differential line width (dLW). This quantity can be considered like the FWHM and carries information about changes in the line width. Its units are m^2/s^2. Pulsations and activity can produce variations in dLW but also can have an instrumental origin. If

the RV signal correlates with the dLW, it is more likely to be due to stellar activity than to a planet.

First, I compute the GLS for the CRX and dLW, which are shown in Fig 13h and i, respectively. There is one significant peak, which has FAP$<$ 10%, at 54.5d in the dLW GLS. There are not other significant periods neither peaks in common between activity indicators and the RVs data and residuals. Also, the Pearson correlation R was calculated for the activity indicators with the RV data and with the residuals from the 16.2d model and there was no correlation, the $|R|$ values were < 0.12. The data were distributed randomly with no visual pattern and the fitted straight lines had small slopes, near to 0.

Due to stars have activity epochs, the activity signature in the full data periodograms may be hidden. For this, instead of using all the data, I compute the GLS using data which are near in time and were obtained during similar stellar activity epoch.

I divided the data in groups. The first one includes the 13 oldest observations from July, 8th 2012 to September, 9th 2012. The second one includes 28 observations from July, 23rd 2013 to January, 6th 2014. The third one collects the archival RVs and the last one includes the 23 new observations.

Only the GLS computed with the activity indicators from the second block of data and the archival data set (in which this second block is) show interesting results but none significant. The GLS of the CRX from the second group of data show two poor defined peaks at $\sim$27.5d and $\sim$36.5d. The archival data confirm their maximums and the $\sim$27.5d get a FAP$\simeq$ 10%. The GLS of the dLW of the second run does not show interesting peaks. The archival data periodogram presents some oscillations between 25d and 36d. One of them is centred at 27.6d and another one at 35.6d but both with FAP$\gg$ 10%. The only significant peak, with FAP$\simeq$ 10%, is centred at $\sim$33d and is clearly separated from 32.4d.

Due to data from the spectroscopic observations with SOPHIE do not present evidences of stellar activity, I search for it in other observations in publicly sky surveys and catalogs.

First, I searched for observations of HD 207897 in ground photometric surveys. The only result was from the All Sky Automated Survey for SuperNovae (ASAS-SN) in which there were about 5 years of data. The light curve of these data looked quiet flat and does not have visual patterns. The periodogram was computed to detect changes in the brightness that could be linked to activity or stellar rotation. The biggest peak is at $\sim$550 days but the most significant one in Figure 11j is at 29.5d. Near the 27.6d line there are the 27.3d and 28d signals but they are clearly separate. Because this surveys observes from ground, data are affected by Moon's phases. The Moon's synodic period is 29.5 days and Moon's sidereal period is 27.3 days. So, the detected signals are related to observational issues and they are not produced by the star.

Then, I checked in VizieR for stellar property catalogs. There are activity indicators, which are calculated directly from spectral lines, such as S-index or $\log R'_{HK}$. $\log R'_{HK}$ measures the chromospheric contribution of the H and K lines of CaII but without the photospheric contribution in these lines and the S-index is also based on H and K CaII lines but it includes continuum's fluxes in the calculations, so it gives information from the chromosphere and the photosphere. These lines are used to characterize the activity because one of the effects of stellar magnetic activity is the enhancement of the emission in these lines' cores.

The chromospheric activity indicators' data were extracted from Boro Saikia et al. 2018 and Isaacson and Fischer 2010. The data from both catalogs are consistent each other and the mean

values are $\log R'_{HK} \simeq -4.8$ and S-index $\simeq$0.22. These values indicate that the star is very inactive, consistent with the previous analyses, that do not find any significant periodicity linked to activity, and is in agreement with the flat ASAS-SN and TESS raw light curves. In addition, Isaacson and Fischer 2010 gives an expected star rotation period of 38 days. I do not trust this value because it has been calculated using only the three S-index points but it is near the ∼37.7d signal in the RV data periodogram (Fig 9*a*).

So, the analyses of the activity indicators do not show a significant evidence of stellar activity in the data. It seems that the observations from July, 23rd 2013 to January, 6th 2014 were taken during a more active epoch of the star compared to the new observations, which are similar in number (23 points) but they have almost flat activity periodograms. The GLS of the CRX and dLW for these active epochs have some peaks in the region of interest and near ∼27d but they are not really significant. The fact that only a part of the data have periodicities that can be interpreted as activity confirms that it is a low-activity star and therefore a long rotation period could be expected. Also, that is consistent with the low values of $\log R'_{HK}$ found in the bibliography. For all that, none of the signals detected in the RVs data can be certainly attributed to stellar activity or rotation.

5.2.4 `juliet` model comparison analysis

The results from the powergram and K analyses are that the unknown signals are not spurious periodicities also there are not evidences that they are produced by stellar activity. Since the residuals' RVs from the 16.2d-period model are about two times its semi-amplitude and their GLS have peaks with FAP$<$ 10%, these invites to explore other possibilities and more complex models. These new models, all based on the original one, are classified into two types depending on how they try to explain the extra signals.

The first one incorporate Gaussian Processes (GPs) with different kernels. The models include already a jitter term prior σ_{instr} as a white-noise model but this simple model may not be the most appropriate. For this, GPs are also introduced for a better approach to the stochastic processes present in data. GP models are evaluated considering circular and elliptical orbits.

The second one are multi-planet models. The significant peaks are treated as Keplerian circular orbits, besides a circular orbit for TOI 1611b.

The explored models are listed in Table 4 with its main features and Bayesian log-evidences referenced to the 16.2d model (Fig. 10). The model's residuals periodograms were computed too. The GLS of the GP model residuals are almost identical to the 16.2d one (Fig. 13*b*) and they are not shown but the multi-planet ones are shown in Fig. 13*c*-*g*. For a better understanding of the model's results, I plot the posterior distribution for the parameters with `corner` package (Foreman-Mackey 2016).

If all the models are equiprobable a-priori, the $\Delta \ln Z_n$ indicates how is the n model more likely than the 16.2d-period model (I used this log-evidence as a reference). A model is clearly favoured in front of another if their $\Delta \ln Z$ is greater than 5. Models are statistically indistinguishable if differences between their lnZ are less than 2. The greater the $\Delta \ln Z$ value, the higher statistical probability.

In the cases that elliptical orbits have been considered, e and ω are fitted using the alternative $\mathcal{S}_1$, $\mathcal{S}_2$ parameterization with uniform priors between -1 and 1. The elliptical models are

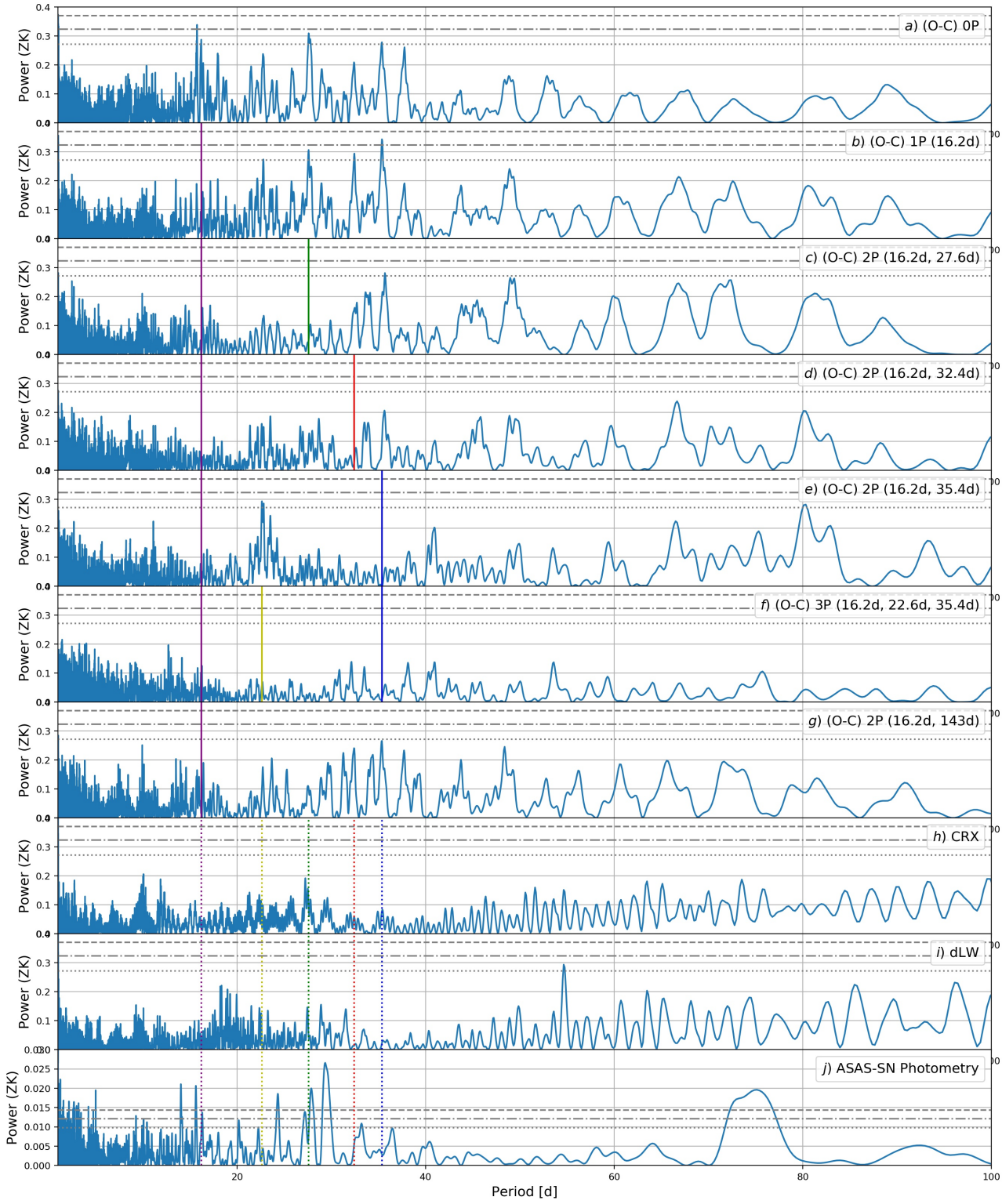

Figure 13: Comparative between generalised Lomb-Scargle (GLS) periodograms for the RV data (a), the residuals after modeling the signals as Keplerian orbits with `juliet` (b-g), the activity indicators chromatic index (CRX, h) and differential line width (dLW, i) and the ASAS-SN photometry (j). Grey horizontal lines indicate the theoretical 10% (dotted), 1% (dash-dotted) and 0.1% (dashed) false-alarm probability (FAP) levels. Color vertical lines indicate the subtracted periods, the dotted ones are only illustrative.

Table 4: Models comparison of RV fits with `juliet`.

Model	Prior P_{planet}	Priors e, ω	$\mathcal{GP}$ kernel	$\Delta \ln Z$
1pl	$\mathcal{N}(16.2009, 0.01^2)$	Fixed (circular)	...	0.00
1pl	$\mathcal{N}(16.2009, 0.01^2)$	$\mathcal{S}_1$, $\mathcal{S}_2$	...	-1.06
1pl+$\mathcal{GP}$exp	$\mathcal{N}(16.2009, 0.01^2)$	Fixed (circular)	Exp$^{(a)}$	10.40
1pl+$\mathcal{GP}$exp	$\mathcal{N}(16.2009, 0.01^2)$	$\mathcal{S}_1$, $\mathcal{S}_2$	Exp$^{(a)}$	9.09
1pl+$\mathcal{GP}$ess	$\mathcal{N}(16.2009, 0.01^2)$	Fixed (circular)	ExpSinSq$^{(b)}$	8.95
1pl+$\mathcal{GP}$ess	$\mathcal{N}(16.2009, 0.01^2)$	$\mathcal{S}_1$, $\mathcal{S}_2$	ExpSinSq$^{(b)}$	7.22
1pl+$\mathcal{GP}$m	$\mathcal{N}(16.2009, 0.01^2)$	Fixed (circular)	Matern$^{(c)}$	9.50
1pl+$\mathcal{GP}$m	$\mathcal{N}(16.2009, 0.01^2)$	$\mathcal{S}_1$, $\mathcal{S}_2$	Matern$^{(c)}$	8.14
2pl	$\mathcal{N}(16.2009, 0.01^2)$	Fixed (circular)	...	0.73
	$\mathcal{N}(27.6, 0.2^2)$	Fixed (circular)		
2pl	$\mathcal{N}(16.2009, 0.01^2)$	Fixed (circular)	...	0.99
	$\mathcal{N}(32.45, 0.2^2)$	Fixed (circular)		
2pl	$\mathcal{N}(16.2009, 0.01^2)$	Fixed (circular)	...	3.86
	$\mathcal{N}(35.5, 0.2^2)$	Fixed (circular)		
3pl	$\mathcal{N}(16.2009, 0.01^2)$	Fixed (circular)	...	5.52
	$\mathcal{N}(22.7, 0.2^2)$	Fixed (circular)		
	$\mathcal{N}(35.5, 0.2^2)$	Fixed (circular)		
2pl	$\mathcal{N}(16.2009, 0.01^2)$	Fixed (circular)	...	3.65
	$\mathcal{N}(143.0, 0.5^2)$	Fixed (circular)		

Notes. The prior label $\mathcal{N}(\mu, \sigma^2)$ represents a Gaussian distribution. $\mathcal{S}_1$, $\mathcal{S}_2$ priors are $\mathcal{U}(-1, 1)$. $^{(a)}$Exponential kernel of the form $k_{i,j} = \sigma^2_{\mathcal{GP},RV} exp(-|t_i - t_j|/\tau_{\mathcal{GP},RV})$. $^{(b)}$Exponential-sine-squared kernel of the form $k_{i,j} = \sigma^2_{\mathcal{GP},RV} exp\left(-\alpha_{\mathcal{GP},RV}(|t_i - t_j|)^2 - \Gamma_{\mathcal{GP},RV} \sin^2\left[\pi|t_i - t_j|/P_{\mathcal{GP},RV}\right]\right)$. $^{(c)}$Matern kernel of the form $k_{i,j} = \sigma^2_{\mathcal{GP},RV} \mathcal{M}(|t_i - t_j|, \rho_{\mathcal{GP},RV})$.

indistinguishable from the circular ones. So, circular orbit models, which are simpler, are preferred.

The GP models are the most likely because their Bayesian evidence values are the highest ones. The most likely no-GP model is the 3-planet model, which has Δ lnZ $\sim$5. There is a a difference of $\sim$5 between the GP and 3-planet models, which is a significant difference. All the GP models are statistically equivalent, the differences between their evidences are less than 2. Despite GP models are the most favored, the 27.6d, 34.4d and 35.5d signals are still present in their residuals with FAP$<$ 10%, even 35d has FAP$<$ 1%.

Eccentric versions of the multi-planet models were computed too but the results were similar to the circular ones and for this are not shown. In addition, I compute a `juliet` fit treating the long-term trend observed at 143d in the RV data as a Keplerian orbit. The residuals' periodogram from this model, shown in Fig. 13*g*, still have the 32d and 35d signals, but non significant. So, this model neither explain the 30's periods.

The two-planet models are in the dubious area of Δ lnZ greater than 2 but less than 5. The multi-planet model with greater evidence is the 3-planet one, probably because it fits the data using three planets instead of two. The residuals' GLS for the 27d, 34d and 35d models are shown in Fig 13*c*, *d* and *e*, respectively. In the residuals of 27d and 32d there is still a clear non-significant peak at 35d. The 35d model is the two-planet model that better subtract these periods, although the 22d signal increases. That peak at 22.6d is the only one significant in the residuals' GLS with

FAP$\simeq$ 10%.

In order to find an explanation to this new period I tried with a 3-planet model. This one is the multi-planet model with greatest log-evidence and its residuals' periodogram (Fig. 13f) does not present high or significant peaks, also because 3 periods are used to fit the data. Nonetheless, the Bayesian log-evidence difference between 3-planet and 35d models is less than 2, that means they are equivalent models.

The models have not been able to explain the periodicities at 27, 32 and 35 days. Despite their residuals are flatter than the GP models ones, their Bayesian log-evidences are very unfavourable. So, I prefer a GP model because are more likely and the signals adjusted in the multi-planet models do not have a clear origin. The Matern kernel model is statistically identical to the exponential one, but this last kernel is simpler. For this, I will use the one-planet GP exponential kernel model to explain the RV data in the joint fit model.

5.3 Photometric and RV fitting model

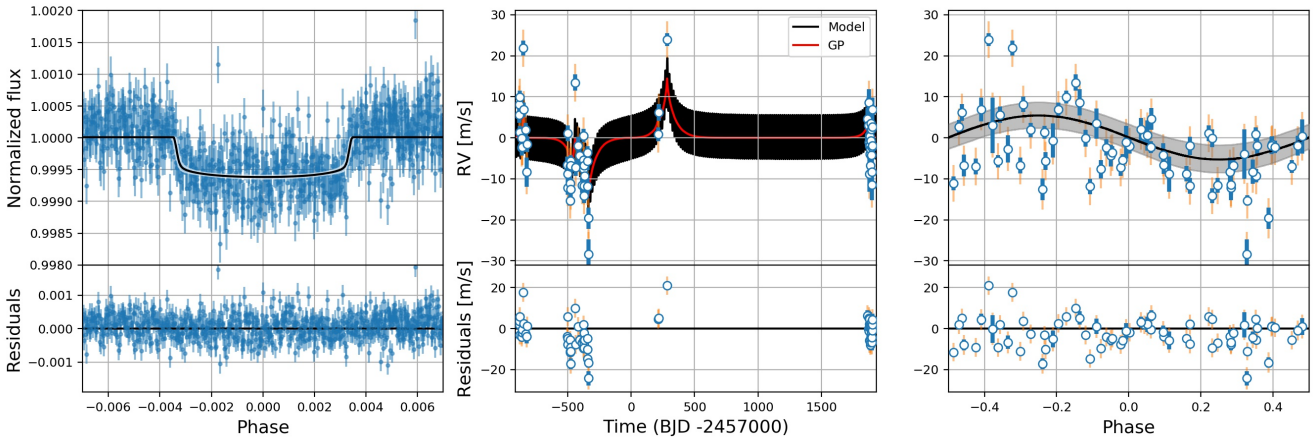

Figure 14: Results from the joint fit of the model 1pl+$\mathcal{GP}$exp. *Left panel*: Phase-folded TESS photometric data (blue dots with error bars) with the transit model (black line). *Middle panel*: SOPHIE RV data (blue dots with error bars) along with the RV model (black line) and the GP (red line). *Right panel*: RVs and the Keplerian component (black line with grey areas denoting the 68% model CI) phase-folded to the joint fit P ($16.2010^{+0.0006}_{-0.0005}$) and t_0 ($1796.4950^{+0.0013}_{-0.0012}$). Orange error bars include the jitter.

After separated analyses of TESS and SOPHIE data, I compute a joint fit of both data with `juliet`. This model constrains simultaneously all the parameters for the transiting planet and the correlated noise in the RV data with an exponential GP kernel. The fit priors and posteriors are shown in Table 6 (*Appendix A*) and the joint model is shown in the Fig. 14.

Using the results from the joint model, TOI 1611b has a M_p=19$\pm$4$M_\oplus$ and R_p=$2.13^{+0.09}_{-0.07}R_\oplus$. The other planetary parameters derived from the `juliet` fit are shown in Table 5. The mass relative error of 21% can be explained by the dispersion and errors of SOPHIE data which has produced a determination of the semi-amplitude with a similar relative uncertainty.

6 Discussion

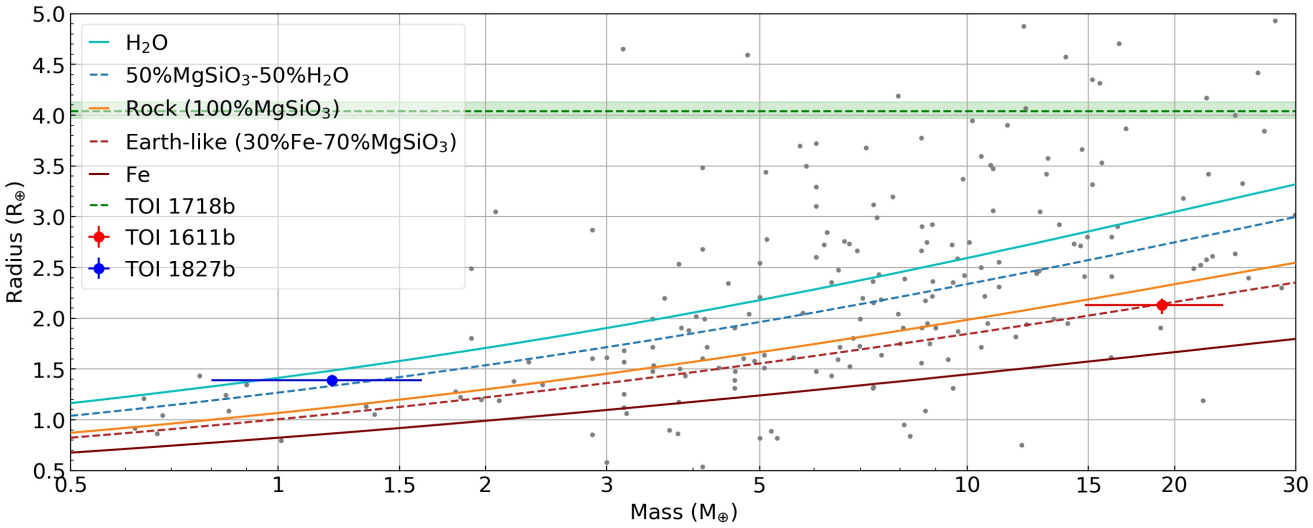

Figure 15: Mass-radius diagram for all the known planets (grey dots) with masses between 0.5-30$M_\oplus$ and radii 0.5-5$R_\oplus$. TOI 1611b (red dot with errors) and TOI 1827b (blue dot with errors) are marked and the green horizontal band denote the radius detection for TOI 1718b. Data are retreived from NASA Exoplanet Archive (`https://exoplanetarchive.ipac.caltech.edu/index.html`). Theoretical two-layer models for internal composition of small planets are taken from Zeng, Sasselov, and Jacobsen 2016.

After analysing TESS Sectors from 17 to 23 and more than 1 000 stars from the RV database, only 3 have shown transit events not related to previously known planets. I computed more complex analyses with `juliet` for these specific targets, TOIs 1611, 1718 and 1827, and from their best fit models I extracted the planetary parameters which are detailed in Table 5.

The first analysed target, for which I could not get RV measurements, is TOI 1718. It was planned to observe it but the weather prevented it. So, I only presented the analysis of its 2-min cadence light curve from TESS. Its four transits caught in Sector 20 are similar and do not seem produced by stellar activity or an eclipsing binary system but without additional data is not possible to certainly confirm it. The planet characterization is not complete and the result of the photometry fit only gives a planetary radius $R_p = 4.04^{+0.09}_{-0.07} R_\oplus$. It is the biggest planet of the three analysed in this work and the hottest one with T_{eq}=1 000$^{+50}_{-21}K$. The other planetary transit parameters are shown in Table 5. For its position in Figure 15, where TOI's radius is marked with an horizontal green line, it seams that it is a gaseous planet like Neptune, which has a similar radius (R_N=3.88$R_\oplus$, M_N=17$M_\oplus$). However, without a mass measurement it is only an assumption.

The second analysed target is TOI 1827. The R_p=1.39$^{+0.06}_{-0.05} R_\oplus$ was extracted from TESS photometry and its errors are one order of magnitude smaller than alerted ones. I have multiple observations from HIRES and HARPS in my database but with big error bars. I get a semi-amplitude of 1.5±0.5m/s from the joint fitting that corresponds to a planet mass of 1.2±0.4$M_\oplus$, yielding a mean density of $\rho_p = 2.4 \pm 0.9$ g/cm^3. But *Trifon Trifonov et al., in prep.* with no-public data from CARMENES has determined a K that is greater than my upper limits. TOI 1827b is

Table 5: Derived planetary parameters obtained for TOI 1611, TOI 1718 and TOI 1827 using the posterior values of their best `juliet` fits.

Parameter[a]	TOI 1611 b	TOI 1718 b	TOI 1827 b
P (d)	$16.2010^{+0.0006}_{-0.0005}$	5.5869 ± 0.0003	1.467144 ± 0.000023
t_0[b]	$1\,796.4950^{+0.0013}_{-0.0012}$	$1\,848.0271^{+0.0005}_{-0.0006}$	$1\,931.1592^{+0.0004}_{-0.0003}$
K (m/s)	5.4 ± 1.2	. . .	1.5 ± 0.5
Derived transit parameters			
$p = R_p/R_\star$	$0.0241^{+0.0010}_{-0.0008}$	$0.0386^{+0.0009}_{-0.0007}$	$0.0376^{+0.0016}_{-0.0014}$
$b = (a/R_\star)\cos i_p$	0.46 ± 0.30	0.31 ± 0.20	$0.48^{+0.25}_{-0.31}$
$a/R_\star$	42^{+5}_{-11}	$14.5^{+0.6}_{-1.3}$	$10.1^{+1.2}_{-2.0}$
i_p (deg)	$89.4^{+0.4}_{-0.8}$	$88.76^{+0.83}_{-1.00}$	$87.3^{+1.9}_{-2.5}$
t_T (h)	$3.3^{+1.7}_{-0.6}$	$3.20^{+0.60}_{-0.25}$	$1.28^{+0.48}_{-0.23}$
Derived physical parameters			
M_p ($M_\oplus$)	19 ± 4	. . .	1.2 ± 0.4
R_p ($R_\oplus$)	$2.13^{+0.09}_{-0.07}$	$4.04^{+0.09}_{-0.07}$	$1.39^{+0.06}_{-0.05}$
ρ (g/cm^3)	11 ± 3	. . .	2.4 ± 0.9
g_p (m/s^2)	41 ± 10	. . .	6.0 ± 2.2
a_p (AU)	$0.155^{+0.017}_{-0.040}$	$0.063^{+0.003}_{-0.006}$	$0.0155^{+0.0018}_{-0.0030}$
T_{eq} [c] (K)	550^{+87}_{-28}	$1\,000^{+50}_{-21}$	875^{+100}_{-47}
S ($S_\oplus$)	15^{+12}_{-3}	166^{+35}_{-14}	49^{+25}_{-10}

Notes.[a]Error bars denote the 68% posterior credibility intervals. [b]Units are BJD-2 457 000. [c]Equilibrium temperatures were calculated assuming zero Bond albedo.

located at the gaseous-rocky region of the mass-radius diagram (Fig. 15) but with CARMENES mass detection (priv. comm.), it migrates to near the rocky composition (100% $MgSiO_3$). Thus, it would be a rocky Earth-size planet at only 8pc with similar surface gravity (g_p from this work is $6.0 \pm 2.2 m/s$) but hotter than Earth, $T_{eq} = 875^{+100}_{-47} K$. TOI 1827b is a very good target for further studies and characterization of super-Earth planets because of the proximity and brightness of GJ 486.

The last and most deeply analysed system is TOI 1611. This was observed by TESS during Sectors 18, 19 and 20 and I get a sum of 67 RVs because the collaboration with the SOPHIE team. This is the only planetary candidate from this work that has been clearly confirmed and for which I performed a full characterization of its properties. Separate `juliet` analyses of photometry and Doppler data detected the signal of a planet orbiting at 16.20 days period and the joint fitting refined the derived planetary parameters, which are detailed in Table 5. TOI 1611b has a mass of $M_p = 19 \pm 4 M_\oplus$ and a radius of $R_p = 2.13^{+0.09}_{-0.07} R_\oplus$. As is shown in the mass-radius diagram (Fig. 15), it is a sub-Neptune sized rocky planet and appears to have a similar composition to that of the Earth according to two-layer models. The RV errors result in large uncertainties over mass detection, 68% CI varies between 15-23$M_\oplus$, more precise observations will be able to narrow its value. Due to its mean density being 11 ± 3 g/cm^3, it seams to have lost its gaseous envelope and no atmosphere is expected to be left.

7 Summary and Conclusions

TESS is observing the northern ecliptic hemisphere and has found more than 300 planetary candidates that are waiting to be confirmed from Sectors 17-23. The strategy applied in this work is to focus on the stars with RV archival data which can be confirmed and characterized without the necessity of performing new observations. For this, I collected archival observations from HARPS, HIRES and HARPS-N and I followed the same methodology in each sector. First, I compute the RV GLS for the observed stars. This allowed to identify the stars with prominent peaks and study if they have already discovered exoplanets. Then, I wait for TESS data. I extract the 30-min cadence photometry for all my targets using `tesseract` and I search for transits in it with `TLS` algorithm. I inspect a hundred light curves in few minutes looking for transits events. But all this procedure is unspecific, it is possible that some star can go unnoticed and I check the TESS Targets of Interest (TOIs) alarms. As a result, I detected the three planetary candidates analysed in this work.

TOI 1718 is an example of the normal case in this field of study, there are too many stars to be all observed with RV facilities. I have not enough Doppler effect measurements to compute a useful periodogram, thus, I only can extract its radius from TESS photometry. For the other two TOIs I had enough RV observations and I could perform joint fits with `juliet`. Despite the RV fit for TOI 1827 not being very precise, I prove that it is a promising super-Earth target for atmospheric characterization. TOI 1611b is the main result of this work and I am writing an article in collaboration with the SOPHIE team. It is a dense sub-Neptune planet with rocky composition around a K0 type star at 28pc that probably has lost its atmosphere.

I detected 3 planetary candidates which is a $\sim$1% of the total alerted. It is a very low rate but almost guarantee the mass detection of an exoplanet in one of the most competitive fields nowadays without the necessity of performing additional observations and only using archival data. TOI 1611b and TOI 1827b contribute to the TESS Level One Science Requirement of finding 50 planets with radii smaller than $4R_{\oplus}$ with measured masses. These discoveries contribute to the change of exoplanetology's main goals from discovering more planets to study them in great detail. That is the only way to one day discover another habitable planet.

References

[1] S. Boro Saikia et al. "Chromospheric activity catalogue of 4454 cool stars. Questioning the active branch of stellar activity cycles". In: 616, A108 (Aug. 2018), A108. DOI: 10.1051/0004-6361/201629518. arXiv: 1803.11123 [astro-ph.SR].

[2] A. J. Cannon and E. C. Pickering. "VizieR Online Data Catalog: Henry Draper Catalogue and Extension (Cannon+ 1918-1924; ADC 1989)". In: *VizieR Online Data Catalog*, III/135A (Oct. 1993), III/135A.

[3] R. M. Cutri et al. "VizieR Online Data Catalog: 2MASS All-Sky Catalog of Point Sources (Cutri+ 2003)". In: *VizieR Online Data Catalog*, II/246 (June 2003), pp. II/246.

[4] Néstor Espinoza, Diana Kossakowski, and Rafael Brahm. "juliet: a versatile modelling tool for transiting and non-transiting exoplanetary systems". In: 490.2 (Dec. 2019), pp. 2262–2283. DOI: 10.1093/mnras/stz2688. arXiv: 1812.08549 [astro-ph.EP].

[5] Daniel Foreman-Mackey. "corner.py: Scatterplot matrices in Python". In: *The Journal of Open Source Software* 24 (2016). DOI: 10.21105/joss.00024. URL: http://dx.doi.org/10.5281/zenodo.45906.

[6] Gaia Collaboration et al. "Gaia Data Release 2. Summary of the contents and survey properties". In: 616, A1 (Aug. 2018), A1. DOI: 10.1051/0004-6361/201833051. arXiv: 1804.09365 [astro-ph.GA].

[7] D. Hidalgo et al. "Three planets transiting the evolved star EPIC 249893012: a hot 8.8-$M_\oplus$ super-Earth and two warm 14.7 and 10.2-$M_\oplus$ sub-Neptunes". In: *arXiv e-prints*, arXiv:2002.01755 (Feb. 2020), arXiv:2002.01755. arXiv: 2002.01755 [astro-ph.EP].

[8] Howard Isaacson and Debra Fischer. "Chromospheric Activity and Jitter Measurements for 2630 Stars on the California Planet Search". In: 725.1 (Dec. 2010), pp. 875–885. DOI: 10.1088/0004-637X/725/1/875. arXiv: 1009.2301 [astro-ph.EP].

[9] Francesco Pepe et al. "HARPS: a new high-resolution spectrograph for the search of extrasolar planets". In: ed. by Masanori Iye and Alan F. Moorwood. Vol. 4008. Society of Photo-Optical Instrumentation Engineers (SPIE) Conference Series. 2000, pp. 582–592. DOI: 10.1117/12.395516.

[10] Keivan G. Stassun et al. "The TESS Input Catalog and Candidate Target List". In: 156.3, 102 (Sept. 2018), p. 102. DOI: 10.3847/1538-3881/aad050. arXiv: 1706.00495 [astro-ph.EP].

[11] L. Tal-Or et al. "VizieR Online Data Catalog: Correcting HIRES/Keck RVs for systematic errors (Tal-Or+, 2019)". In: *VizieR Online Data Catalog*, J/MNRAS/484/L8 (Nov. 2018), J/MNRAS/484/L8.

[12] Lev Tal-Or et al. "Correcting HIRES radial-velocities for systematic errors". In: *European Planetary Science Congress*. Sept. 2018, EPSC2018–862.

[13] Trifon Trifonov et al. "A public HARPS radial velocity database corrected for systematic errors". In: *arXiv e-prints*, arXiv:2001.05942 (Jan. 2020), arXiv:2001.05942. arXiv: 2001.05942 [astro-ph.EP].

[14] S. S. Vogt et al. "HIRES: the high-resolution echelle spectrometer on the Keck 10-m Telescope". In: ed. by David L. Crawford and Eric R. Craine. Vol. 2198. Society of Photo-Optical Instrumentation Engineers (SPIE) Conference Series. 1994, p. 362. DOI: 10.1117/12.176725.

[15] M. Zechmeister and M. Kürster. "The generalised Lomb-Scargle periodogram. A new formalism for the floating-mean and Keplerian periodograms". In: 496.2 (Mar. 2009), pp. 577–584. DOI: 10.1051/0004-6361:200811296. arXiv: 0901.2573 [astro-ph.IM].

[16] M. Zechmeister, A. Reiners, et al. "Spectrum radial velocity analyser (SERVAL). High-precision radial velocities and two alternative spectral indicators". In: 609, A12 (Jan. 2018), A12. DOI: 10.1051/0004-6361/201731483. arXiv: 1710.10114 [astro-ph.IM].

[17] Li Zeng, Dimitar D. Sasselov, and Stein B. Jacobsen. "Mass-Radius Relation for Rocky Planets Based on PREM". In: 819.2, 127 (Mar. 2016), p. 127. DOI: 10.3847/0004-637X/819/2/127. arXiv: 1512.08827 [astro-ph.EP].

Appendix A

Table 6: Prior and posterior parameters of the final joint fit model 1pl+$\mathcal{GP}exp$ for the analysis of TOI 1611b using `juliet`.

Parameter	Prior	Posterior[(a)]	Description
		Stellar parameters	
$\rho_\star$ (kg/m^3)	$\mathcal{L}(100, 10^4)$	$5\,400^{+1\,900}_{-3\,000}$	Stellar density
		Planet parameters	
P (d)	$\mathcal{N}(16.2009, 0.01^2)$	$16.2010^{+0.0006}_{-0.0005}$	Period
$t_0^{(b)}$	$\mathcal{N}(1\,796.495, 0.1^2)$	$1\,796.4950^{+0.0013}_{-0.0012}$	Time of transit-center
K (m/s)	$\mathcal{U}(0, 20)$	5.4 ± 1.2	RV semi-amplitude
r_1	$\mathcal{U}(-1, 1)$	$0.64^{+0.19}_{-0.20}$	Parametrization for p and b
r_2	$\mathcal{U}(-1, 1)$	$0.0241^{+0.0010}_{-0.0007}$	Parametrization for p and b
$\mathcal{S}_1$	0.0 (fixed)		Parametrization for e and ω
$\mathcal{S}_2$	0.0 (fixed)		Parametrization for e and ω
		Photometry parameters	
D_{TESS}	1.0 (fixed)		Dilution factor
σ_{TESS} (ppm)	$\mathcal{L}(0.1, 10^3)$	315.4 ± 1.8	Extra jitter term
$q_{1,TESS}$	$\mathcal{U}(0, 1)$	$0.15^{+0.23}_{-0.11}$	Quadratic limb-darkening parametrization
$q_{1,TESS}$	$\mathcal{U}(0, 1)$	$0.30^{+0.38}_{-0.22}$	Quadratic limb-darkening parametrization
		RV parameters	
μ_{SOPHIE} (m/s)	$\mathcal{U}(-50, 50)$	11 ± 3	Systemic velocity
σ_{SOPHIE} (m/s)	$\mathcal{L}(0.1, 100)$	$4.1^{+0.8}_{-0.9}$	Extra jitter term
		GP hyperparameters	
$\sigma_{\mathcal{GP},RV}$ (m/s)	$\mathcal{L}(0.1, 100)$	61^{+24}_{-21}	Amplitude of GP component
$\tau_{\mathcal{GP},RV}$ (d)	$\mathcal{L}(10^{-4}, 10)$	$0.016^{+0.038}_{-0.010}$	Length-scale of GP component

Notes. The prior labels $\mathcal{N}(\mu, \sigma^2)$, $\mathcal{U}(min, max)$, $\mathcal{L}(min, max)$ represent normal, uniform and log-uniform distributions. Parametrization $\mathcal{S}_1 = \sqrt{e}\sin\omega$ and $\mathcal{S}_2 = \sqrt{e}\cos\omega$, ensuring that $e = \mathcal{S}_1^2 + \mathcal{S}_2^2 \leqslant 1$. [(a)]Error bars denote the 68% posterior credibility intervals. [(b)]Units are BJD-2 457 000.